UCRL-TR-228713

LAWRENCE
LIVERMORE
NATIONAL
LABORATORY

Understanding and Improving High Voltage Vacuum Insulators for Microsecond Pulses

J.B. Javedani, D.A. Goerz, T.L. Houck,
E.J. Lauer, R.D. Speer, L.K.Tully,
G.E. Vogtlin, A.D. White,

March 06, 2007

Disclaimer

Auspices Statement

This work was performed under the auspices of the U. S. Department of Energy (DOE) by the University of California, Lawrence Livermore National Laboratory (LLNL) under Contract No. W-7405-Eng-48. The project 06-ERD-033 was funded by the Laboratory Directed Research and Development Program at LLNL.

Table of Contents

List of Figures

FY06 LDRD Final Report

Understanding and Improving High Voltage Insulators For Microsecond Pulses

LDRD Project Tracking Code: 06-ERD-033

J. B. Javedani and D. A. Goerz, Principal Investigators

Abstract

High voltage insulation is one of the main areas of pulsed power research and development, and dielectric breakdown is usually the limiting factor in attaining the highest possible performance in pulsed power devices. For many applications the delivery of pulsed power into a vacuum region is the most critical aspect of operation. The surface of an insulator exposed to vacuum can fail electrically at an applied field more than an order or magnitude below the bulk dielectric strength of the insulator. This mode of breakdown, called surface flashover, imposes serious limitations on the power flow into a vacuum region. This is especially troublesome for applications where high voltage conditioning of the insulator and electrodes is not practical and for applications where relatively long pulses, on the order of several microseconds, are required.

The goal of this project is to establish a sound fundamental understanding of the mechanisms that lead to surface flashover, and then evaluate the most promising techniques to improve vacuum insulators and enable high voltage operation at stress levels near the intrinsic bulk breakdown limits of the material. The approach we proposed and followed was to develop this understanding through a combination of theoretical and computation methods coupled with experiments to validate and quantify expected behaviors.

In this report we summarize our modeling and simulation efforts, theoretical studies, and experimental investigations. The computational work began by exploring the limits of commercially available codes and demonstrating methods to examine field enhancements and defect mechanisms at microscopic levels. Plasma simulations with particle codes used in conjunction with circuit models of the experimental apparatus enabled comparisons with experimental measurements. The large scale plasma (LSP) particle-in-cell (PIC) code was run on multiprocessor platforms and used to simulate expanding plasma conditions in vacuum gap regions. Algorithms were incorporated into LSP to handle secondary electron emission from dielectric materials to enable detailed simulations of flashover phenomenon. Theoretical studies were focused on explaining a possible mechanism for anode initiated surface flashover that involves an electron avalanche process starting near the anode, not a mechanism involving bulk dielectric breakdown. Experiments were performed in Engineering's Pulsed Power Lab using an available 100-kV, 10-μs pulse generator and vacuum chamber. The initial experiments were done with polyethylene insulator material in the shape of a truncated cone cut at +45° angle between flat electrodes with a gap of 1.0 cm. The insulator was sized so there were no flashovers or breakdowns under nominal operating conditions. Insulator flashover or gap closure was induced by introducing a plasma source, a tuft of velvet, in proximity to the insulator or electrode.

I. Introduction / Background

Pulsed power, the compression of energy in both space and time, is a critical technology area for many nuclear weapons science, national security, defense, and industrial applications. Pulsed power technology is often employed to create extreme states of matter for high-energy-density-physics and hydrodynamics experiments, and enables many types of scientific apparatus such as high-current particle-beam

accelerators, high-power radiofrequency and microwave sources, high-power laser sources, pulsed neutron sources, nuclear weapons effects simulators, lightning and electromagnetic pulse effects simulators, x-ray and proton radiography machines, inertial fusion drivers, directed energy weapons, and electromagnetic launchers.

High voltage insulation is one of the main areas of pulsed power research and development, and dielectric breakdown is usually the limiting factor in attaining the highest possible performance in pulsed power devices. For many applications the delivery of pulsed power into a vacuum region is the most critical aspect of operation, and the past two decades have seen a sustained growth in the diversity and complexity of devices where vacuum is required to support high voltages and high electric fields.

The surface of an insulator exposed to vacuum can fail electrically at an applied field more than an order or magnitude below the bulk dielectric strength of the insulator. This mode of breakdown, called surface flashover, imposes serious limitations on the power flow into a vacuum region. While many researchers have studied this problem over several decades, there is still no consensus of opinion about the underlying mechanisms that fully explain this phenomenon [1]. The goal of this project is to establish a sound fundamental understanding of the mechanisms that lead to surface flashover, and then evaluate the most promising techniques to improve vacuum insulators and enable high voltage operation at stress levels near the intrinsic bulk breakdown limits of the material.

Some of the earliest studies of surface flashover discovered that conical shaped insulators exhibit surface flashover at higher electrical field thresholds than do cylindrically shaped insulators. Figure 1 shows the dependence of the flashover field on the angle of cone shaped acrylic insulators. Cones with positive angles (larger base against cathode electrode) generally withstand higher fields than do cones with negative angles [2].

One of the more surprising properties of surface flashover is that it can be initiated at either the cathode or anode end of an insulator, and that the breakdown mechanisms in these two cases appear to be distinctly different. In either case, however, the surface flashover can occur on a nanosecond time scale, which rules out any explanation requiring the transit of ions across the inter-electrode gap.

Cathode initiated surface flashover is thought to be initiated by electrons field emitted from the cathode which strike nearby regions of the insulator with enough energy to eject more electrons, resulting in a net positive surface charge which presumable becomes large enough to draw secondary electrons back to the surface, creating an avalanche of electrons that propagates towards the anode [3]. The prevailing theory explains that by increasing the angle of the insulator, there is a reduced likelihood of an electron emitted from the cathode surface striking the insulator and causing secondary electron emission.

Conical shaped insulators with positive angle have the attribute that the electric field in the vicinity of the cathode triple junction (CTJ), where the electrode, insulator, and vacuum all meet, is reduced while the electric field in the vicinity of the anode triple junction (ATJ) is increased. Modeling shows that a positive 45-degree angle on an acrylic insulator reduces the electric field at the CTJ.

Insulators having positive angles and proper electrode shaping to sufficiently reduce the electric fields at the CTJ and/or surface coatings on the electrode to suppress electron emission, thus avoiding cathode initiated surface flashover will, at some higher level, eventually experience anode initiated surface flashover.

The breakdown mechanism of anode initiated surface flashover is different from cathode-initiated flashover and is less well researched or understood. Unlike cathode-initiated flashover which results in minimal damage to the insulator, anode-initiated flashover produces a dense, widely branching, tree-like pattern of micron sized grooves on the insulator surface as shown in Figure 2. Note that if the driving circuit energy is too low, then there will not be enough energy in the system to cause the insulator any noticeable damage, although the insulator can still experience flashover from an anode initiated event. A damaged insulator degrades the ability of the insulator to repeatedly achieve the same voltage hold-off. The anode-initiated surface flashover has been observed to propagate from anode to cathode, opposite in direction to the cathode-initiated mechanism, but with comparable speed [4]. Not all anode initiated breakdowns as we have found out and will explain in this report are bulk breakdown.

Micro-protrusions or whiskers on the electrode in the vicinity of the cathode triple junction could significantly enhance the local electric field causing electron field emission leading to surface flashover. This problem seems to be so prevalent that we devoted a significant effort of our experimental campaign investigating this mechanism behind insulator breakdown.

Another type of high-voltage vacuum insulator that has been devised primarily for accelerator applications is the so-called micro-stack insulator that is composed of multiple thin alternating layers of dielectric and metallic materials bonded together. This type of insulator is thought to somehow disrupt or suppress the secondary electron avalanche process, allowing it to operate at higher electrical stress levels than conventional insulators [5]. There is interest in this type of insulator for particle accelerator applications because it could possibly enable higher field gradients and also be in close proximity to the beam line, which has advantages for power flow impedance matching and suppression of beam-breakup instabilities [6]. Although testing has been done to evaluate performance levels and determine scaling for various structures, the exact mechanism that may be governing performance is not yet fully understood [7]. The work we have done was to add secondary electron emission physics to an existing PIC (particle-in-cell) code to study the effect of the secondary electron avalanche on conventional insulators can be expanded to study the underlying mechanism of voltage hold off of the so-called high gradient insulators.

Insulators with non-traditional shapes have been utilized in a limited number of applications [8], but not enough scientific analysis and experiments have been done to demonstrate their ultimate performance levels or limitations. We hope that the fundamental understanding and methodology gained from this project can be expanded and applied to investigate the behavior of these innovative insulators.

II. Research Activities

Current best practices in high voltage insulator design have evolved over several decades and have been based primarily on empirical results without the benefit of substantial computational studies. The approach we have proposed and followed is to develop a thorough understanding of the fundamental mechanisms governing surface flashover of high voltage vacuum insulators using computational methods coupled with experiments to validate and quantify expected behaviors.

Our plan has been to model and test insulator designs that will reduce the electric field stress at the cathode and anode triple junctions to evaluate and characterize their ability to suppress surface flashover. We have examined designs that incorporate raised electrodes in close proximity to the edge of the insulator material as well as raised electrodes imbedded inside the dielectric material. Various shapes have been explored to determine effectiveness at reducing the magnitude of the electric field at the critical junction region, while also examining the impact of modifying the direction of electric field along the insulator surface. There is still great controversy among experts in the field as to which matters the most, reduced field stress or steepness of field direction, at the critical junction region. Based on field modeling and particle trajectory modeling we are striving to determine the optimal shapes necessary to maximize expected voltage hold-off, and then perform experiments to validate predicted performance improvements and sensitivities. As we gain greater understanding, we will be able to explore novel shapes, such as contoured edges, and examine their expected performance in comparison to conventional angled insulators.

Eventually we will need to model and test insulators with a variety of defects introduced during manufacturing that are postulated to create field enhancements sufficient to induce surface flashover. Gaps between the insulator and electrode surfaces, whiskers on the insulator surfaces, and micro-protrusions on the electrodes should all be evaluated, first with modeling and subsequently with experiments. Our approach was to do sufficient parameter studies to cover the range up to assured flashover and strive to ascertain an acceptable threshold of imperfection that a workable design can have.

II.A. Modeling, Simulation and Theoretical Effort

Computational and analytical studies were used to set directions and agenda for meeting the objectives of the project, and to support the project at several levels. Initial efforts were directed towards modeling possible mechanisms for insulator breakdown or flashover. These efforts evolved into designing experiments and the required diagnostics to verify the mechanism models. Finally, the results of the experiments were analyzed and compared to the models. In practice the studies, design efforts, and comparisons often occurred in parallel with the experiments as data provided better information on which to base improved models. Several specialized commercial codes were used in the computational and analytical studies. A listing and description of the more commonly used codes is provided in Section II.A.1.

We developed flowcharts to describe the mechanisms of both cathode-initiated and anode-initiated breakdown phenomena. These proposed mechanisms for insulator flashover represent reasonable explanation for the behavior observed by others and ourselves. This phenomenology is presented in Figures 3 and 4.

Generally speaking, cathode-initiated surface breakdown can result from explosive emission of electrons from either 1) micro-protrusions on the electrode when average electric fields are >100 kV/cm or 2) dielectric fibers, whiskers, lint, and debris when average electric fields are <100 kV/cm.

Anode initiated breakdown can be the result of the high stress that is placed at the ATJ from the applied electric potential that either 1) causes bulk breakdown due to ohmic heating, or 2) causes surface breakdown due to a whisker at the ATJ. The commonly observed treeing effect is a variance of bulk breakdown that happens under a thin layer of the insulator, starting from the anode and is not attributed to ohmic heating, since the path is not always fully traversed to the cathode.

An important observation made during our experimentation was that insulator flashover could occur where the initiating event was located at the anode triple junction but did not involve bulk breakdown of the dielectric. We hypothesize that an electron avalanche, where the origin of the avalanche starts near the ATJ but then propagates towards the cathode, is the prevailing mechanism in this mode of anode initiated breakdown. Our proposed theory for this “reverse propagating avalanche” is presented in Section II.A.5.

II.A.1. Principle Computational Tools

Specialized software was required to meet the analytical and computational needs of this project. A short description of each code we utilized is given below:

Microcap™ - A Spice-based circuit modeling code having an integrated schematic editor and mixed analog and digital simulator that provides an interactive sketch and simulate environment for electronics engineers. This code is a product of the Spectrum Software Inc.

Maxwell™ - 2D & 3D finite element method electromagnetic design software for the simulation and analysis of electromagnetic components. This code is a product of the Ansoft Corporation. Field modeling was performed with both Maxwell 2D and 3D version to examine geometrical effects.

TriComp™ and AMaze™ Suites of software or simply Trak and OmniTrak include 2D & 3D conformal mesh generators, finite element electrostatic field solvers, and charged particle optics. This suite of codes is a product of the Field Precision, LLC. As we progressed to examine finer details related to manufacturing defects we determined that these codes, primarily due to the zoom-in option described below, were a better set of computational tools to use.

Mathematica™- A numerical and symbolic programming code suited for solving mathematical functions with graphics system. This code is a product of Wolfram Research.

LSP™ - A 3D time dependent, electromagnetic particle-in-cell (PIC) code designed for large scale plasma simulations. This is an open source code and runs in parallel on multiple CPUs on Linux based computers. The code is a product of ATK Systems Corp.

Lumped circuit element codes such as Microcap™ were needed to determine the characteristics of the power delivered to the electrodes separated by the insulator. The information from a circuit code was then used with an electrostatic solver like Maxwell™ to determine electric field stresses on the insulator and adjacent electrodes. Estimates of the system capacitance and sizing of the electrodes to avoid edge effects are examples of electrostatic solver usage.

For a conservative design of a non-critical insulator, this level of design and analysis may be sufficient. The next level of design effort considers the possibility of field emission and plasma formation. Charged particle optics codes permit the study of the electron orbits and the affect of external electric and/or magnetic fields, e.g. magnetic insulation. Codes such as Tricomp and Amaze suites of codes are used at the stage of analysis. These codes are time independent providing the steady state solution. However, in most electrode configurations the movement of free electrons is on a time scale that is much faster than other phenomena, e.g. plasmas. In this case a reasonable approximation is to use the time independent code repeatedly to generate a "movie" of snapshots. This quasi-time dependent data can then be incorporated into a circuit code. This is a relatively sophisticated level of design.

To accurately model the breakdown and or flashover of the electrode/insulator requires a fully electromagnetic, time dependent, particle-in-cell code such as LSP™. The simulation difficulty is further increased as a breakdown is a fully 3D phenomenon. Significant computational resources are needed. All of the design steps mentioned in the preceding paragraphs must be used to narrow the scope of the problem to be simulated. Also, the required physics for the simulation needs to be considered, e.g. will secondary electron emission, back scattering, gas desorption, UV induced photoelectrons, etc. be a consideration. The more physics included, the longer the simulation and the greater the possibility of an incorrect solution. The size of the problem can necessitate examining small sections of the overall problem and extrapolating.

II.A.2. Examples of Field Modeling

Two codes were used at this level of modeling; Maxwell and Tricomp/Amaze Suites of codes are simply referred to in this report as Trak. Both codes are finite element method (FEM) electrostatic solvers and have 2D and 3D capabilities. Figures 5 and 6 show the Maxwell ™ capability of the electrostatic solver for calculating electric fields for several cases of interest. Figure 5 shows the electric field and the electric equipotential lines for a one-quarter section model of the base case of the test insulator in 3D for an applied voltage of 100 kV. Figure 6 shows the results of 2D modeling along a line drawn slightly above the cathode for; 1) an ideal insulator with no interface gap with cathode, 2) a defective insulator with a notched gap as the interface and 3) a cathode bump to lower the field locally at the cathode triple junction (CTJ).

Trak has the special feature of an automated zoom option; see Appendix 1 – which was used to generate the solutions presented in Figure 7. This is a 3D analysis of the extreme filed enhancements possible from micro-protrusions in the shape of thin needles with semispherical tips (radius of 1.0 μm and length of 1000 μm) placed at the CTJ and ATJ. The fields on the needle tip reach extremely high values of 3.96E+05 kV/cm at the CTJ and 10.81E+05 kV/cm for the ATJ case.

Appendix 2 discusses the results when the material property of the needle in Figure 7 is switched from a perfect electric conductor (PEC) to a fiber with dielectric constant ε of 2.80. In this case, the tip of the fiber near the CTJ has a maximum field value of 172 kV/cm, whereas the tip of the fiber near the ATJ has a

maximum filed value of 332 kV/cm for 100 kV applied across a 1.0 cm gap. Some degree of polarization is evident in both fibers.

According to a paper by R.B. Miller on Mechanism of Explosive Electron Emission for Dielectric Fiber Cathodes [9], the characterization polarization time of dielectric fibers is about 90 ns and 16 kV/cm of field is required to cause surface breakdown along the length of the fiber. The analysis presented in Appendix 2 is electrostatic, but it is a correct treatment since the risetime of our voltage pulse is about 180 ns on samples of velvets as will be discussed in the experimental section.

The ability to finely resolve critical features of possibly small defects in rather large problem spaces is important in studying insulator flashover mechanisms. We explored the limit on accuracy for calculating the magnitude of electric field and potential in the triple point region of the insulator/vacuum interface. We did this using the TriComp electrostatic solver with its zoom feature, and then compared and validated the results to an analytical approach. It can be shown mathematically that the field increases as $r^{-\nu}$ approaching the ATJ and decreases as r^{ν} approaching the CTJ for a positive insulator angle where r is the distance to the respective triple junction and ν is a positive number [10], [11]. Appendix 3 gives more details about this evaluation and analytical validation. A brief summary is given below:

The high resolution modeling shows that the field strength in the vicinity of the ATJ for +100 kV across a 1.0-cm gap with a +45 degree insulator (ε = 2.8) does increase to extremely high values as the ATJ approached. With finite element codes, the limitation on how close one can get to zero distance away from either of the triple junctions depends on the size of the local mesh. The highlights of the finding for two different mesh sizes of 30 μm and 0.2 μm are given below:

Mesh Size, μm	$\|E\|_{ATJ}$, kV/cm	$\|E\|_{CTJ}$, kV/cm
30.0	280	47
0.2	612	21

For the case of 0.2 μm, several zoom steps were used in order to reach this level of resolution. This level of zoom is impressive, when compared to insulator length of 1.0cm (a ratio of 1 to 20,000). At 0.2 μm mesh, for this size problem, we are at the verge of the double precision accuracy of the computer. The results of this work have been documented and will be presented at the 2007 IEEE Pulsed Power Conference [12].

II.A.3. Example of Combinational Circuit Modeling

The lumped element circuit code MicroCap, was initially used to predict pulser performance with resistive loads. In order to model plasmas i.e., velvet as the load, Trak (charged particle optics software in the TriComp Suite) and Microcap were used in combination. Trak was used to give the expected Child-Langmuir currents of an ideal expanding hemispherical plasma as a function of position within the gap - see Figure 8. The results were then read into Microcap in a table as a function of time and a comparison between the experiment and modeling was done. Appendix 4 shows the modeling steps done with Trak and Microcap to enable comparison with experiments. The comparison shows verification that the measured current is truly due to space charge limited flow from an expanding hemispherical plasma and the code has been benchmarked by the experiment.

II.A.4. Examples of LSP Simulation Modeling

Our LSP simulations were performed on a relatively small (34-cpu) Linux cluster supported by the Beam Research Program and Engineering. Later, we successfully ran LSP on a larger (4096-cpu) LC server. Below we describe four general types of simulations performed with LSP:

1) Simulation of velvet emission

Electron emission from the plasma generated by a velvet dot on a bare electrode, i.e. no insulator, was simulated in 2D cylindrical coordinates – for comparison with experiments see section II.B.5.1. The velvet/plasma source was modeled as a 2 mm diameter, 1 mm tall neutral plasma cylinder composed of equal parts electrons and protons. The number density was varied from 10^8 to 10^{12} particles/cm^3 and the protons were given an initial temperature of 0.05 to 0.1 eV. Reference [9] was used for estimating physical values for the plasma. Figure 9 shows the simulated geometry and a close up view of the typical particle movement at three separate simulation times. The red macro particles represent proton and green represent electrons. The simulation included a LCR circuit model to drive the electrodes and a threshold voltage applied to the cathode under/near to the plasma to model the adhesive tape on the back of velvet-dots. The simulations were typically performed using 5 cpu's and 100 ns simulation time took 24 hours.

The simulations reached a quasi-steady state within a few nanoseconds after the field had increased to 20 kV/cm. The envelope of electron orbits and the current was changing slowly. For this time scale the protons had not moved appreciatively. After a few tens of nanoseconds the simulation would become unstable due to oscillations of the positive macroparticles. The instability could be delayed somewhat by going to smaller time steps and a finer grid, but the time to run the simulation increased dramatically. Three of the more important results of the simulations were:

1. The current and expansion of the electron orbits crossing the gap agreed with the Trak results and our experiments.
2. Varying the threshold voltage for cathode emission simulated the first pulse delay on a new velvet-dot in the experiments, confirming the hypothesis that the delay was due to the insulating layer of adhesive attaching the velvet to the cathode.
3. Varying the location of and threshold voltage for emission from the cathode with respect to the plasma produced orbit patterns consistent with the results of Y.M. Saveliev and W. Sibbett [13].

2) Simulation of velvet under a radial step and charging of the insulator

An important question about fabrication and assembly of vacuum insulators is the tolerance required for locating the insulator between the electrodes. Specifically, how much concern should there be with small gaps between the cathode electrode and the insulator, and do such gaps increase the probability of plasma generation and flashover at the CTJ. Figure 10 illustrates the geometry used in the simulations and experiments to address this question. The initial belief was that the electric field in the gap is enhanced increasing the likelihood and amount of field emission from debris on the cathode surface and/or the cathode itself. Simulations were performed with LSP to study this hypothesis and the effect of space charge from the emitted current and possible charging of the insulator.

The problem was modeled in 2D cylindrical coordinates. A LCR circuit model was used to drive the electrodes. The circuit was slightly mismatched to the impedance of the insulator/electrode geometry leading to a "stair stepped" charging of the electrodes as shown Figure 10b. A space charge limited emission region was placed on the cathode surface under the insulator. The simulation shown in the figure took 12 hours, using 12 cpu's.

The results were unexpected, but confirmed by experiment (see section II.B.5.2.). Electrons leaving the cathode are deposited on the underside of the insulator canceling the electric field in the gap. The plot at the bottom of Figure 10c shows electrons in blue leaving the cathode. The smaller graph on the plot shows the extracted current as a function of time. This current is simply the derivative of the applied voltage pulse. As the voltage is increased, current is extracted that is deposited on the insulator. As the voltage reaches an intermediate step, the deposited charge cancels the field in the gap and the emission stops. This is analogous to displacement current when charging a capacitor. The plot shows orbits at a minimum current time. Electrons are stagnating in the gap and a few are being deflected towards the CTJ and away from the insulator. Gaps or crevices between the insulator and cathode seem not to be critical issues by themselves. However, further modeling that includes photoelectron physics might be warranted. The sole

issue may be the trapping of debris at the CTJ. And, there remains the issue that debris in the vicinity of the CTJ might likely be a serious problem.

3) Simulation of a secondary electron emission

The production of secondary electrons is an important phenomenon for various models of insulator flashover. The LSP code was modified to add a module that created secondary electron emission (SEE). This is a separate phenomenon from backscatter electrons which occurs at much higher energies. Figure 11 shows the geometry and some results of the SEE simulations. We used 2D cylindrical coordinates with a constant ramp voltage to 14 kV over 0.4 ns. For the reduced axial geometry shown, a 5 ns simulation could be performed in less than 2 hours using 6 cpu's.

For the simulation shown, an intermediate electrode was placed in the dielectric insulator. The primary particles (blue) were generated by space charge limited emission at the CTJ. Incident particles striking the dielectric material will generate secondary particles (green) based on a probability yield matrix involving energy and angle. Those particles striking the electrode generate secondary particles (red) from a different probability yield matrix.

The simulation did result in a cascading of secondaries along the surface. Over the dielectric material, an equilibrium condition would develop where the insulator would develop a slight negative charge that would keep particles orbits from intercepting the surface. This effect limits the growth of the avalanche. To demonstrate a true flashover, the simulations need to incorporate physics models that allow for the desorption and ionization of a neutral gas.

4) Simulation of electron avalanche from CTJ with angled insulator in 3D

Our most ambitious simulation is a 3D representation of or an electron avalanche originating at the CTJ of an angled insulator. Even for a reduced geometry where the electrodes are spaced only 0.5 mm apart, a 1 ns simulation time takes 10 hours using 20 cpu's. For our present status of trouble shooting the simulation physics, this is a manageable situation. But as we attempt to increase the same of the problem, it will be necessary to expand to several hundred cpu's or more. Figure 12 shows results at the beginning of emission (top) and about 0.03 ns into the pulse when current is almost fully established. Both side and front views of the simulation are shown.

A few secondaries (red) are produced at the edge of the emission site, but these electrons follow the primary beam across the gap and do not avalanche across the surface. Future efforts will include varying the angle of the insulator from the perpendicular to determine the point where an avalanche is no longer sustained and looking at the effect of charge deposits on the insulator surface. From experiments, we know that the insulator will flashover as soon as an expanding plasma touches the surface. Thus, we are looking at the physics that is not included in the simulation to understand the missing mechanism.

II.A.5. Future Modeling and Simulation Challenges:

We have successfully demonstrated particle emission including secondary electron emission, charging of dielectrics, and space charge effects on orbits. Physics phenomena that we are beginning to explore include desorption/ionizing of neutrals, UV induced photoemission, SEE emission from an angled insulator, and initial charge deposits on the insulator. More important, we are developing the ability to simulate the electron avalanche model proposed by E.J. Lauer, with this time-dependent PIC code (see section I.A.6.).

II.A.6. A New Theory of Electron Avalanche from ATJ

We have observed breakdowns that appear to have originated from the anode, but do not appear to involve bulk breakdown of the dielectric. We surmise that an electron avalanche starting near the anode is the mechanism. However, the onset of the avalanche cannot start with the original electric field that is in a

direction that will pull electrons from the dielectric surface towards the vacuum. An initiating event has to occur near the anode to produce enough positive charge on the surface of the dielectric to reverse the direction of the electric field normal to the dielectric surface, E_n. Field emission results in positive surface charge, but it is self-limiting and turns off before E_n reaches zero. The initiating event might be field emission from a whisker with ohmic heating vaporizing the whisker followed by electron ionization and collection of the electrons at the anode. Such an event is most likely in the enhanced electric field near the anode triple junction.

Once a positive surface charge capable of reversing the localized E_n has been created, electrons that leave the dielectric near this charge will be attracted towards the surface. These electrons may leave the surface due to field emission or photoionization. They are the components of the first surface avalanche. In order for the following avalanches to step toward the cathode, the positive surface charge after a series of avalanches must change E_n from repulsive to attractive upstream (towards the cathode) of the location of the original surface charge.

A simple analysis of electron orbits can be made by assuming that E_n and E_t are constant over the orbit. Refer to the figure to the right for orientation of the coordinate frame, u and v, with respect to the dielectric. We can then analyze the normal and tangential motion separately. Consider a single electron released from the surface at u_o with energy U_0. The electron will move a distance v_o from the surface in a time t. The tangential component of the electric field will cause the electron to move a distance l along the surface before it impacts with an energy U.

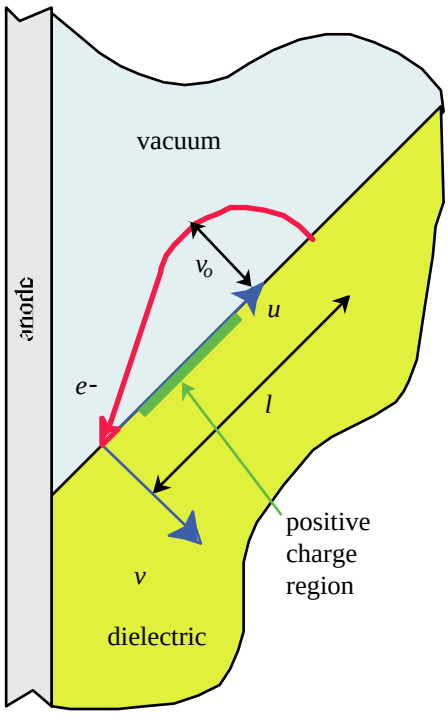

$$U_0 = eE_n v_0 \qquad v_0 = \frac{eE_n}{2m}\left(\frac{t}{2}\right)^2$$

$$l = \frac{eE_t}{2m}t^2 = \frac{2U_o}{e}\frac{E_t}{E_n^2} \qquad U = U_0 + elE_t = U_o\left(1 + 2\frac{E_t^2}{E_n^2}\right)$$

We will now consider $n[u]$ electrons moving in the negative u direction and an equal number of immobilized positive ions that are distributed at the positions where they were formed. The change in n along the surface can be expressed as

$$-\frac{\partial n}{\partial u} = n\frac{(\sigma - 1)}{l} = d$$

Where σ is the secondary electron coefficient and d is the line density of positive ions. We can now write down an interactive method for solving for the electric field as the avalanche progresses. E_{ti} and E_{ni} are the fields at u_i. E_{tpi} and E_{npi} are the fields before the avalanche starts.

$$E_{ti} = E_{tpi} - \frac{2}{\varepsilon + 1}\sum_j \frac{\Delta d_j}{(\Delta i - \Delta j)^2} \qquad E_{ni} = E_{npi} - \frac{2}{\varepsilon + 1}\sum_j \frac{\Delta d_j\, v_c}{\left[(\Delta i - \Delta j)^2 + v_c^2\right]^{3/2}} \qquad t = \frac{(4mU_0)^{1/2}}{eE_n}$$

The remaining terms give the field at u_i due to the positive ion distribution generated in previous steps of the present avalanche. Δ is the step size in u. The sums over j are cut off at j = i – k where kΔ is the cut-off distance from the head of the avalanche, v_c is the average distance of the charge inside the dielectric, t is the time for a single step.

The images of the ion charges in the anode are neglected because they are much farther from u than the nearest ions.

To use this model, we first assume a localized, positive charge distribution in the insulator surface near the ATJ. A 3D electrostatic code is then used to calculate the fields, E_t and E_n from the applied voltage and the charge. Next, a Mathematica™ script is used to solve the equations for a time step and determine the new charge distribution. The 3D electrostatic code calculates the new fields, E_t and E_n. This iterative process is repeated to step the avalanche across the insulator. Eventually we would like to incorporate this procedure into a time dependent PIC code such as LSP™.

This work is fully explained in a UCRL report, and is being submitted for publication [14].

II.B. Experimental Campaign

The goal of our experimental effort was to characterize a number of different mechanisms that could possibly cause flashover along the insulator/vacuum interface [15]. We considered many options, of which the following three seemed most applicable; first a material defect was introduced to the electrodes or insulator such as the step beneath the insulator previously discussed. Second, introduce a micro-protrusion in form of a small needle as has been done previously by others [4]. Third, introduce a small piece of dielectric material as the electron/plasma source.

As we began planning for our experimental work, we faced the reality that we needed to devise a means to induce flashover at modest stress levels in order to consistently produce results with the relatively low voltage (100 kV) pulser we had available. Following the suggestion of George Vogtlin, we began our experimentation using tufts of velvet, to represent a generic mechanism to introduce explosive emission of electrons. Velvet is widely used in the accelerator community as a high current electron beam emitter for pulsed radiography applications. In this approach small pieces of velvet are inserted at various locations on the cathode, the anode, or even the insulator to study how plasma expansion causes gap closure in form of the insulator flashover. The mechanism of explosive electron emission of velvet is well known; plasma is formed via surface flashover along the length of the velvet fibers when electric field stresses exceed threshold as low as 16 kV/cm [9].

Our initial experiments characterized the plasma generated by placement of a velvet-dot (1.0 mm in diameter) on the cathode surface without the presence of the insulator. This effort provided development and testing of diagnostics. The data also validated the design of the experiment and early modeling. Testing of insulators with velvet generated plasma followed. Note that the production and expansion of plasma on the cathode surface is a critical problem. Whether the plasma expands directly across the electrode gap or across the cathode surface to the insulator, the system will experience a catastrophic voltage collapse. Techniques such as anodizing, polishing, cleaning and/or “conditioning” the cathode surface are used to raise the threshold field for plasma production. Experiments have indicated that if flashover from the cathode is successfully suppressed the region at or near the ATJ will become the limiting factor [15], [16].

II.B.1. Experimental Apparatus

A high voltage test stand for vacuum insulator studies was designed and constructed in Engineering's Pulsed Power Laboratory. The test stand is comprised of a vacuum chamber, high voltage pulser, and electrode fixtures for insulator testing. The vacuum of the chamber is maintained with a cryogenic pump (CTI – Cryo-Torr 8 cold head) with a pumping speed for air of 1500 liters/s. Testing was done at pressures of less than 5 micro-torr. The vacuum chamber is shown in Figure 13.

The applied voltage was generated by a variable voltage 500 J, 100 nF capacitive discharge unit (CDU) that incorporates a triggered spark-gap series switch, waveform shaping components, a triggered spark-gap crowbar switch, and a coaxial cable output. The CDU is capable of producing up to 100 kV voltage pulses of 180 ns rise-time with a pulse-width up to 10 μs into a resistive load. The grounded cathode was the lower plate with a current transformer around the supporting stalk. A 250 ohm resistor in series with the CDU output was used to limit the maximum current. Normally the crowbar is activated after 5 μs. Spacing between the electrodes was nominally set at 1.0 cm. The pulser is based on a design originally developed for the Heavy Ion Fusion Injector for LLNL’s re-circulating induction accelerator [18], [19]. See Figure 14.

II.B.2. Electrodes, Dielectric and Surface Preparation

Electrodes were aluminum with a 32 micro-inch finish. For some of the experiments, the cathode was anodized in accordance with MIL-A-8625C to produce a type III (hard), Class-1 (non-dyed) coating with a

specified thickness of 0.002 - 0.004 inches. The cathode diameter was 15.0 cm and the anode diameter was 10.0 cm.

Two different dielectric materials were used for the insulator: HD polyethylene and polycarbonate (Lexan). The overall load capacitance (with the nominal HD polyethylene insulator) can be calculated from displacement current measurements (peaks at 45 Amp, for 100 kV CDU charge) to be about 17 pF. The insulators were machined to a 32 micro-inch finish. The Lexan insulator was vapor polished after machining to produce a clear surface. A transparent surface is important for viewing the "tree" pattern associated with ATJ initiated breakdowns.

II.B.3. Velvet Tuft as the Electron Emitter

In many of the tests, small pieces of synthetic velvet were used to facilitate flashover. Three different types of velvet were tested; two were Lucia brands used at the LLNL FXR accelerator for the field emission cathode. The third brand selected, made by Double Eagle (black in color) was found the most reliable at "lighting off", i.e. forming plasmas at the lowest field stress. We were able to obtain explosive electron emission initially at 80-100 kV/cm levels and after conditioning at 40-60 kV/cm levels, so it became the velvet of choice [20]. The velvet was nominally cut with a circular base of 1 mm diameter, a height of about 1.5 mm, and was comprised of about six tufts of fibers. The velvet was then attached to the surface with a small dot of double stick tape (3M, # 465 light industrial, adhesive transfer type). Figure 15 shows a velvet-dot positioned near the CTJ of an HD polyethylene insulator.

II.B.4. Diagnostics

A liquid resistive voltage divider attached to the drive cable at the entrance to the vacuum chamber monitored the output of the CDU. The voltage monitor was fabricated at LLNL and calibrated in situ against a commercial high voltage probe. The current was measured with a Pearson 110 current transformer installed around the cathode support stalk. Both of these monitors are relatively slow (~20 MHz bandwidth), although sufficient for the plasma studies. For future experiments, we plan to install D-dot probes with sub-nanosecond response in the cathode (at ground potential) under the insulator.

We also fabricated an anode that consisted of a thin foil of aluminum backed by a scintillating plastic (BC422). As sketched in Figure 16, the back of the anode can then be imaged with a framing camera to determine the distribution of electrons striking the anode. The camera used for this purpose was a high resolution intensified CCD camera (PI-Max) to image the scintillation of the BC422 due to electrons extracted from the expanding plasma [21]. The camera setup on the chamber is shown in Figure 17.

II.B.5. Measurements and Observations

Before installation of the velvet on the cathode electrode, the voltage hold off of the bare Aluminum electrodes with 1.0 cm gap was tested at +100 kV and 5 μs long CDU pulses. There were no breakdowns in this configuration. We then proceeded with the velvet-only test in order to characterize the velvet/velvet generated plasma. The insulator was then introduced to the configuration. Placement of the velvet-dot in the vicinity of the CTJ and of the ATJ followed. We also experimented with placing the velvet-dot on the insulator. A fresh velvet-dot was installed at the beginning of each series. Normally each shot was repeated 3 times for the velvet-only and velvet-dot at the CTJ cases. The turn-around time between shots was ~10 minutes. For the velvet-dot at the ATJ series, the shots were repeated as many as 10 times.

Unless specifically noted, all the tested insulators were HD Polyethylene, truncated 45^{o} cones, 1.0 cm thick, and the base of the cone has a diameter of 6.0 cm. The velvet-dot was 1.0 mm diameter, 1.5 mm thick of the Double Eagle brand and black in color.

The list of tested configurations were: 1) Velvet-dot only, 2) Velvet-dot in the vicinity of CTJ, 3) Velvet-dot at ATJ, 4) Velvet-dot on the insulator and 5) Velvet-dot at ATJ of a thinner Lexan insulator.

Below a summary of key measurements and observations that were made in each shot series is given:

1) Velvet Only:

The first velvet test was performed with an electrode spacing of 1.0 cm without an insulator to determine the field level of the velvet "light-off", i.e. explosive generation of plasma. Figure 18a shows that the velvet-dot was placed at a radially offset position. This "zero" offset position is where the CTJ would be, if there were an insulator. Figure 18b shows typical oscilloscopes traces of the voltage and current signals. The first pulse on a newly installed velvet-dot would occasionally hold voltage for over 1.0 μs at 100 kV before lighting off. On subsequent pulses the "light-off" would usually occur during the rise time for CDU charge voltages as low as 60 kV. At 40 kV charge, the velvet "light-off" was delayed or did not occur.

The displacement current provided a time fiducial for the applied voltage and current pulses. Also, the electron transit time across the gap was less than 200 ps for the experiment configuration. Thus, the velvet "light-off" can be determined to within about 1 ns from the onset of current and droop in voltage. Complete voltage collapse occurs at plasma closure permitting an estimate of the plasma velocity, ~ 2.58 cm/μs in the example shown in Figure 18b.

After installation of the framing camera, we were able to verify the transverse velocity by capturing images shown in Figure 19. The cross section of the expanding plasma is circular and remains circular until it makes contact with the anode. From the difference between the gate-widths and the diameter of the circular spot a velocity ~ 2.0 cm/μs was inferred – not taking into account the jitter time at the time of trigger.

It was not clear from this experiment if the plasma expansion was hemispherical about the light off position. The answer to the question was inferred from subsequent testing (described in more detail in the next section) where the velvet was placed at various distances from the CTJ.

2) Velvet-dot in the Vicinity of CTJ:

Prior to placement of velvet at the insulator's CTJ, the HD Polyethylene insulator was placed in the gap and tested, and as expected, the 1.0 cm thick sample held off +100 kV, 10 μs pulses repeatedly without any problems.

Next, velvet-dots were placed at different distances from the insulator to determine the plasma transverse velocity and effect on the insulator. The distances of the 1.0 mm diameter velvet-dots were 0.0 mm, 2.0 mm, 4.0 mm and 6.0 mm from the CTJ when measured from the closest edge. Voltage and current waveforms are shown in Figure 20 for an applied voltage of +80 kV at different positions.

In reporting this data please note that in these cases; 1) the shots were done on a "conditioned at 100 kV" piece of velvet and 2) the insulator had some charge built up due to the prior shots that can affect the timing of the velvet light off and 3) of the three shots taken for each velvet location the signals have been adjusted in time so that the velvet "light-off" is consistent.

In this series of shots the voltage collapse time is on the order of a few ns, which is too fast to be resolved with the relatively slow (20 MHz bandwidth) diagnostics. Note also that the plasma velocity varies from shot to shot, although, there does not appear to be a trend for greater plasma velocity with increased voltage. Plasma velocities ranging from 1.5-2.75 cm/μs were observed. The data does indicate a slowing of expansion with distance. An important result was that UV from the plasma did not cause the insulator to flashover prior to plasma arrival. If this had not been the case, then the time scale at which the flashovers took place would have been independent of the distance of the velvet-dot position from the CTJ to the accuracy of our measurements.

Results from this test indicated that there was a decrease in average velocity as the velvet was placed further from the insulator and as the plasma expanded. The average velocity for the plasma to cross the gap (vertical velocity) was greater than the average transverse velocity for the same distance of expansion which would indicate that the vertical plasma expansion did not slow as quickly. Thus, the expansion is only approximately hemispherical.

Experimental results indicate that once the plasma is emitted from the velvet, it expands somewhat hemispherically until it reaches the insulator. This was verified with CCD camera images. Upon contact with the insulator the voltage collapse is eminent. Figure 21 shows the images taken with the CCD camera for this situation. The faint light that is seen on the cathode at every frame is reflected light from the insulator. The orientation of the reflective electrode surfaces with respect to the viewing angle results in this reflected image having the same orientation as if the insulator was viewed directly. The increased intensity of the light near the anode triple junction was not expected. To resolve the time evolution of this light, we have considered using an intensified streak camera in the next campaign.

In addition to the velvet-dot tests describe above, we experimented with insulator "defect". The defect was created by placing a radial step (1.5 mm x 1.5 cm) in the insulator. See Figure 22a. First the insulator was pulsed without a velvet-dot under the step. The insulator held voltages up to +60 kV but flashed at an applied voltage of +80 kV with some > 1 μs delay on the first shot, and did not flash again.

Recall that the nominal insulator, i.e., without the step, held charge at 100 kV without any problems. The radial step in the insulator lowered the voltage hold off to 60 kV. This is a critical finding for a single shot event. Not enough pulses were done to draw any conclusions on how the radial step would have affected the voltage hold off if it was "conditioned".

The shot series was then repeated with the velvet-dot under the step at 60 kV and the geometry held the voltage for all the 3 shots for 5 μs, as it did for the case of no velvet. See Figure 22b for voltage waveforms. No distinction could be made between the two cases of with and without velvet. The expectation was that the velvet would "light-off" earlier or at a lower voltage due to the increased field in the gap, the plasma would then expand under the insulator to the CTJ, and the insulator would flashover. The results did not make sense, until simulations with LSP indicated that initial electrons from the velvet would charge the insulator canceling the electric field in the radial step and preventing light-off. See section II.A.4. and Figure 10.

3) Velvet-dot at ATJ:

Next, we performed tests with the velvet-dot placed adjacent to the ATJ of the HD polyethylene insulator. With velvet at this location, insulator flashover occurred consistently at +100 kV with (0.2 μs, 0.9 μs and 0.2 μs) delay, see Figure 23, and broke less consistently at +80 kV. However, there were no signs of any damage to the insulator.

We expect to see "tree" like damage tracks along the insulator surface where flashover had been induced. When no tracks were observed, we changed the experimental configuration to: 1) replace the HD polyethylene insulator with one made of Lexan and having a smooth finish and 2) replace the velvet-dot with a ring of velvet that was sandwiched between the insulator and the anode electrode. The velvet ring caused consistent flashover on the voltage rise. Still, there was no noticeable damage to the transparent Lexan insulator after 10 shots. The breakdown appears to take place on the surface and not in the bulk. This may suggest that the electron avalanche theory discussed in section II.A.6 is applicable; however, more testing at higher energy levels should also be done.

Of the 500 Joules of CDU's stored energy, the portion that is transferred to the insulator during voltage collapse under the worst condition is calculated to be only ~ 0.1 Joule. The low energy available to sustain the arc is a likely explanation for absence of the treeing effect.

For the velvet-dot (and not the velvet ring) at the ATJ, we also captured several CCD camera images. Figure 24 shows these images. Because of lesser light intensity, no neutral density filters were used. A narrower and fainter light is seen reflected on the cathode. Again, the light appears to originate from the ATJ and propagate across the insulator towards the cathode.

4) Velvet-dot on the Insulator:

Placing velvet on the insulator surface resulted in a delayed (1.6 to 4.8 μs) flashover at 100 kV charge and no flashover at 80 kV charge. When the insulator did flashover, the current/voltage signals were similar to placing the velvet at the CTJ. This response may have a similar cause as the first pulse "light-off" delay noted for the velvet-dots on the cathode. In both cases an insulating layer limits the flow of electrons through the velvet fibers. Once the adhesive between the velvet-dot and the cathode has been "punctured" this barrier is gone and early "light-offs" can occur. In the case of the velvet-dot on the insulator surface, the barrier remains.

5) Velvet-dot at the ATJ of a Small Lexan Insulator:

In this configuration the electrode spacing was reduced to 3.0 mm and polished Lexan insulators with a clear surface finish were tested. This provided stronger electric fields for the same applied voltages. An anodized cathode was used in this test configuration to ensure that the cathode did not inadvertently produce stray electrons. With no insulator, the 3 mm gap could consistently hold off pulses from the CDU charged to +80 kV (i.e., 266 kV/cm). As before, we proceeded with placement of a velvet-dot at the ATJ of the insulator. At +80 kV, there was a flashover of the insulator after 3.5 μs. Repeat shots gradually reduced the voltage hold off drastically. After 10 shots this configuration could only hold off about 40 kV before collapsing on the voltage rise. See Figure 25. Again, there was no noticeable damage to the bulk of the transparent insulator.

To put the reported electric field (voltages) above in perspective, a summary of key electric field magnitude for the discussed cases above is given in Table1.

Table 1: Electric field values specific to certain event or geometry.

	Case	Electric Field, 'kV/cm"	Comments
1	**Velvet-dot Only**	60	Velvet is on the cathode. The first conditioning shot is at 100 kV. The velvet then lit off consistently at 60 kV and randomly at 40 kV.
2	**Velvet-dot at CTJ**	60	Conditioned velvet lit off consistently at 60 kV and randomly at 40 kV, the same as in case 1.
3	**Velvet-dot at ATJ**	100	Field of 100 kV/cm was needed to light off the velvet at ATJ. Light off was not possible at +80 kV. Compare this case to case 2.
4	**Velvet-dot on Insulator**	100	Same as in case 3.
5	**Radial Step Under Insulator**	60	Voltage hold off was 60 kV. Compare this case to case 2. Inserting a velvet dot in the gap did not affect the voltage hold off.

From Table1, it can be concluded that the threshold field for plasma formation at the CTJ is 60 kV/cm and at the ATJ is 100 kV/cm. It can be argued for the velvet at ATJ that there is enough of a field gradient along the length of 1.2 mm long fibers for the velvet to emit. For the sake of completeness it would have been better if we had data from velvet-dot on the anode (without the insulator). It is not clear why the velvet should emit in this configuration even at 100 kV/cm but if it did then it would merit further investigations with simulations.

II.B.6. Summary of Observation made with CTJ initiation:

Key observations of what was inferred from above measurements for the velvet-dot at the CTJ are as follows:

1) Plasma and not the UV from the plasma has been the culprit in causing insulator flashover. If this had not been the case, then the time scale at which the flashovers took place would have been independent of the distance of the velvet-dot position from the CTJ and would have been much faster.
2) The velvet only case shows a speed of 2.58 cm/μs (100 kV charge) across the gap once it is conditioned. The current is no longer Child Langmuir limited and increases steeply after the plasma arrives or is launched at the CTJ.
3) Breakdown takes place with no precursor voltage droop or current for the velvet placed at the CTJ. The reproducibility of this phenomenon was consistent. The electrons that are pulled out of velvet glide along the surface of the insulator freely at time scales too fast to be measured by our relatively slow probes. The 20 MHz bandwidth (17.5 ns risetime) of the voltage and current probes can not help us understand how rapidly surface flashover progresses.
   Glock in his thesis has measured this closure time to be 3 ns across a 1.78 cm, $+45^{o}$ insulator, equivalent to 2.38 ns across our insulator which is the time required for an "avalanche" of charge to move across the insulator [22]. In comparison, calculation shows that the transit time of a lone electron across a 1.0 cm gap for voltages of interest is >1.0 ns. See Appendix 5.
4) The plasmas produced by velvet-dots at 2.0, 4.0 and 6.0 mm away from CTJ show average velocities of 2.25, 1.75, and 1.55 cm/μs along the cathode. This data indicates that plasma slowed down as it expanded. See also Figure 26. The vertical velocity of the plasma across the gap was greater than the average transverse velocity for the same distance of expansion which would indicate that the vertical plasma expansion did not slow as quickly. Thus, the expansion was only approximately hemispherical, as shown for the example case of velvet-dot at 4.0 mm away in Figure 27. Also data suggests that no strong correlation between plasma velocity and the breakdown voltages existed. See Figure 28.
5) The "defect" that was put in place on the insulator in the form of a radial step lowered the voltage hold off of the insulator from 100 kV to 60 kV. The velvet-dot in the gap beneath the insulator did not affect the voltage hold off of the "defective" insulator. This would imply; 1) that gaps should be avoided in insulator-cathode interface and 2) the existence of lint or debris inside the gap, does not affect the already lowered voltage hold off. However, lint or debris adjacent to the CTJ most likely would.
6) From CCD camera images, it is not clear, if the 1.0 mm diameter velvet lights off from the edges or its center. The CCD camera images did not have sufficient spatial resolution to determine this. The faint light that is seen on the cathode at every frame is reflected light from the insulator (see Figure 21). Although not conclusive, the intensity distribution of the reflected light would suggest the ATJ as the origin.

II.B.7. Summary of Observation made with ATJ initiation:

Key observations of what was inferred from above measurements for the velvet-dot at the ATJ are as follows:

1. None of the breakdowns at the ATJ can be attributed to bulk breakdown since there were no observable damages (e.g., treeing effect) to the insulator. - The amount of energy transferred from the CDU to the insulator during the ATJ initiated flash over is only about 0.1 Joule. This is probably not enough energy deposition to cause permanent damage.

2. The anode initiated breakdowns that we observed were all surface breakdowns, induced by the presence of the velvet. To our knowledge no one has reported on this mechanism for breakdown. The mechanism of electron avalanche leading to surface flashover from the CTJ is a classically known phenomenon [3], [23] but the notion of a similar mechanism of electron avalanche leading to surface flashover from the ATJ is very new. It is not intuitively obvious why the electrons initiated at the ATJ would not just get absorbed in the neighboring anode and would instead avalanche on the surface of insulator making it to the cathode. We have developed a theory that explains this mode of breakdown as discussed in section II.A.6.
3. Breakdowns on the first few shots of a newly installed velvet occurred with a time delay (less than 1 μs). The breakdowns would happen on the voltage rise after these preliminary shots. Replacing the velvet-dot with a velvet ring caused breakdown on the voltage rise every time.
4. The voltage collapse is too fast to be resolved by either of the voltage or current probes in any of these discharges. Faster response probes are needed to collect accurate data.
5. The faint light that is seen on the cathode at every frame is reflected light from the insulator (see Figure 24, lower left frame). Although not conclusive, the intensity distribution of the reflected light would suggest the ATJ as the origin. Use of a streak camera to resolve the direction the light propagates on the surface is needed.

III. Exit Plan

This LDRD project was originally envisioned to be a two-year effort. In the first year we planned to perform extensive modeling and specific experiments to understand the fundamental mechanism responsible for initiation of surface flashover. In the second year we planned to extend the modeling to the more challenging 3D particle-in-cell analysis to further study secondary electron avalanche phenomenon, and exhaustively examine the influence of insulator geometry and surface properties on flashover conditions. Furthermore in the second year, we planned to incorporate more sophisticated electrical and optical diagnostics into the experimental test stand and then perform controlled experiments to examine surface flashover phenomenon, validate computational analysis, and finally evaluate methods and designs to mitigate flashover and achieve higher performance with better designed high voltage vacuum insulators.

We completely achieved our first year's objectives, and this report summarizes those accomplishments. In planning for the second year, however, there were certain circumstances that caused us to be concerned about achieving our next year's goals within reasonable schedule.

First, key players on the project team were oversubscribed with programmatic work demanding higher priority. Second, the Pulsed Power Laboratory, where the experimental test stand resides, was under renovation, which shut downed the experimental work for the last quarter of FY06 and at least the first quarter of FY07. Third, licenses and technical support for the LSP code to run on the LC server were held up because of corporate changes and legal matters.

Given these circumstances, the principle investigators requested that the project be suspended for a year. In the interim period before this projects resumes several meaningful activities and related efforts will set the stage for resumptions and successful completion of this project.

First, all of the project team members will continue to apply and enhance their special expertise in programmatic support in related areas. Second, the experimental test stand will be maintained in the Pulsed Power Laboratory, and used for programmatic work and related techbase projects. Third, the LSP code licenses and technical support contacts will be provided and maintained for programmatic support. Forth, two techbase projects were proposed and sponsored through strategic mission support for energy manipulation technologies. One project will develop the faster electrical diagnostics necessary to study the onset and development of flashover phenomenon, the other project will investigate and quantify the effects of UV exposure that may contribute to vacuum insulator flashover.

IV. Summary

High voltage vacuum insulators are important to many applications of pulsed power for scientific experiments and national security programs. Surface flashover imposes serious limitation on power flow into vacuum regions. This project served to develop a fundamental understanding of the mechanisms that lead to surface flashover. Computational, experimental and theoretical studies were accomplished to meet the objectives of this project.

Our modeling and simulation efforts included applications and extension of many configuration tools including the Microcap™, Maxwell™, TriComp™, AMaze™, and LSP™ codes. Field modeling examined and quantified the resolution possible for simulation field enhancements and possible defect mechanisms. Circuit modeling was used in combination with plasma codes to compare experimental results. Particle-in-cell modeling was used to simulate and study the plasma physics at play in the mechanisms leading to onset of insulator flashover.

We assembled a high voltage test stand for vacuum insulator studies with the minimal set of diagnostics to perform our initial experiments. We opted to use velvet tufts to represent possible defect materials and be a plasma source for experimentation at relatively low field stress levels. We performed experiments on traditional typed of insulators made from polyethylene and polycarbonate. Our measurements and observations support the theory that surface flashover starting near the cathode triple junction is triggered by explosive electron emission from a nearby micro-protrusion or dielectric whisker/debris. Our

experiments to examine flashover starting near the anode triple junction did not produce residual tree-like damage patterns, most likely due to insufficient energy in the discharge.

Our theoretical studies led to a description and supporting analysis of a possible mechanism for anode initiated surface flashover that involves an electron avalanche process starting near the anode, not a mechanism involving bulk dielectric breakdown.

To that end, a small operational experimental test facility was built here at LLNL. At the facility, we mocked experiments to induce flashover on conventionally shaped (i.e., +45 degree) insulators by the aid of an embedded plasma source. The plasma source in these experiments is a small (1.0 cm in dia.) piece of a synthetic velvet that goes through explosive emission at relatively low fields (i.e., >40 kV/cm). After some characterization testing of the velvet, we experimented with placing the velvet-dots at different locations of the insulator; cathode triple junction, anode triple junction of the insulator and the insulator itself. Based on our observations, a phenomenology chart of various breakdown mechanisms was put together. Surprisingly, we stumbled upon a mode of anode initiated breakdown, as evident in CCD camera images and current and voltage waveforms that is unique to all relatively low in energy systems and is explainable by a theory that was developed by the theoretician on the project, E.J. Lauer, well in advance of the experimental observation

This research throughout has enjoyed strong computational support. State of the art commercial finite element electromagnetic codes and particle-in-cell (PIC) codes were used in increasing our understanding of the flashover phenomenon. The finite element codes were used in design of the test chamber and the time dependent PIC code LSP™ has the correct physics to handle space charge of the expanding velvet plasma and the secondary electron emission of plastic insulators.

The events leading to a flashover might be long (~ 1.0E-06 seconds) but the flashover of the insulator itself happens at much faster times (~1.0E-09 seconds). Faster diagnostics are being fabricated and purchased to resolve the flashover time. The data taken by the fast probes will be used to benchmark the PIC code.

Acknowledgments

We greatly appreciate the assistance of Gregory Hawkins and James Crawford with assembling the vacuum system and constructing the experimental apparatus. We also would like to thank Tony Ferriera for his help in developing the HV pulser, Mike Ong and the FXR project team for the loan of the CCD camera, and Paul Wargo of NSTec for his expertise and help in operating the camera.

References

1) R.A. Anderson, “Surface Flashover: Three Decades of Controversy.” 14th International Symposium on Discharges and Electrical Insulation in Vacuum, Santa Fe, New Mexico, September 1990.

2) O. Milton, "Pulsed Flashover of Insulators in Vacuum," IEEE Transactions on Electrical Insulation, Vol **7**, No. 1, March 1972.

3) K. D. Bergeron, "Theory of the Secondary Electron Avalanche at Electrically Stressed Insulator-Vacuum Interface," Journal of Applied Physics, Vol. 48, No. 7, July 1977

4) R. A. Anderson, “Anode Initiated Surface Flashover,” 1978 Annual Report of the Conference on Electrical Insulation and Dielectric Phenomenon, 1979.

5) J. M. Elizondo, "Novel High Voltage Vacuum Surface Flashover Insulator Technology," 15th International Symposium on Discharges and Electrical Insulation in Vacuum, Darmstadt,1992.

6) W. R. Cravey, "Investigation of a High Voltage Vacuum Insulator for the DARHT Accelerator," Proceeding of the 11th IEEE Pulsed Power Conference, pp. 555-558, 1997.

7) S. E. Sampayan, et al., "High Gradient Multilayer Insulator Technology," Proceedings of the 2004 Power Modulator Conference, San Francisco, CA, 2004.

8) M. J. Wilson and D. A. Goerz, “Method for Improving Performance of Highly Stressed Electrical Insulating Structures,” US Patent 6340497.

9) R.B. Miller, “Mechanism of explosive electron emission for dielectric fiber (velvet) cathodes”, Journal of Applied Physics, Volume 84, Number 7, 1 October 1998, pp. 3880-3889

10) M.S. Chung, B-G. Yoon, P.H. Cutler, and N.M. Miskovaky, “Theoretical analysis of the enhanced electric field at the triple junction”, J VAc Sci Tech B 22(3), May/June 2004.

11) M.S. Chung, T.S. Choi, B-G. Yoon, “Theoretical analysis of the field enhancement in a two-dimensional triple junction”, Applied Surface Science, 2005.

12) L. K. Tully, et al. “Electrostatic Modeling of Vacuum Insulator Triple Junctions,” UCRL-TR-227505, 2006.

13) Y.M. Saveliev and W. Sibbett, “Current conduction and plasma distribution on dielectric (velvet) explosive emission cathodes,” Journal of Applied Physics, Vol. 94, No.12 Dec 2003, pp. 7416-7421.

14) E. J. Lauer, “Electron Avalanche Model of Dielectric –Vacuum Surface Breakdown,” UCRL-TR-(pending) 2007 for submission.to Journal of Applied Physics for publication.

15) T.L. Houck, “Study of Vacuum Insulator Flashover for Pulse Lengths of Multi-Microseconds”, Linear Acceleration Conference, Knoxville, TN, USA, August 21-25, 2006.

16) G. E. Vogtlin, “Insulator Breakdown Measurements in a Poor Vacuum and Their Interpretation,” LLNL, UCRL-JC-103450, June 1990.

17) W.A. Stygar, et al., “Improved Design of a High-Voltage Vacuum Interface, Phys. Rev. ST Accel. Beams 8050401 (2005)

18) M Hernandez, et. al. “Technologies for Advanced Induction Accelerators,” Project ID 97-ERD-086, LDRD Annual Report FY 1997, UCRL-LR-113717-97.

19) M. Wilson, et. al. “HIF Impulse Injector Design, Construction, and Checkout,” UCRL-ID-130764, 1998

20) Matt Myers of NRL (Elektra Facility) shipped us with the Double Eagle Brand velvet.

21) Princeton Instruments PI-MAX CCD filmless Gen II (UV-Blue) Intensifier Camera.

22) W.R. Glock, Masters Thesis, Cornell University, 1969.

23) H.C. Miller, In “High Voltage Vacuum Insulation”, Edited by R. V. Latham, Chapter 8, Academic Press, 1995. ISBN: 0-12-437175-2

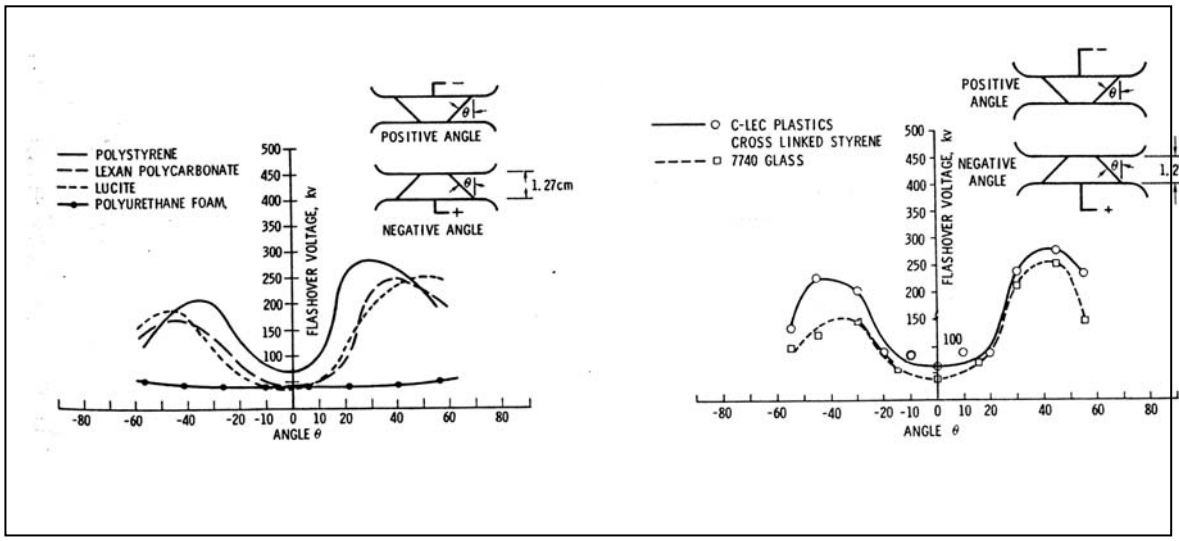

Figure 1: Flashover voltage vs. insulator angles for a few dielectrics from Milton [2].

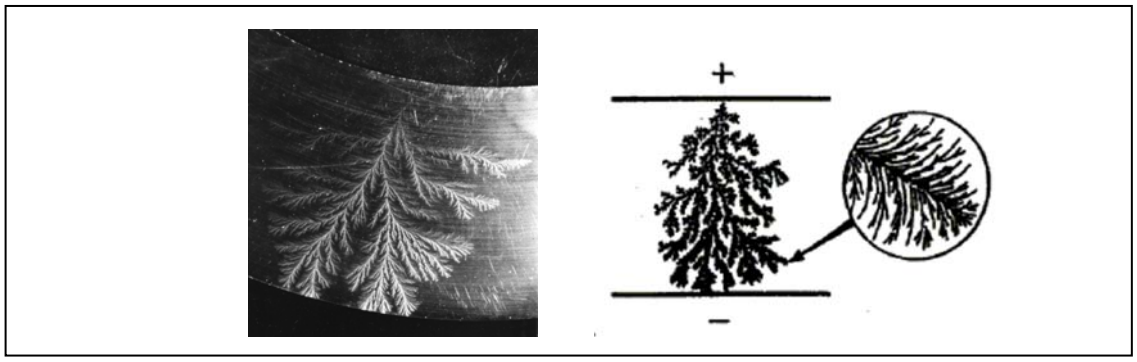

Figure 2: Appearance of the surface damage resulting from a single anode-initiated flashover on a polymeric insulator. Photo is courtesy of G.E. Vogtlin.

Cathode Initiated Surface Breakdown:

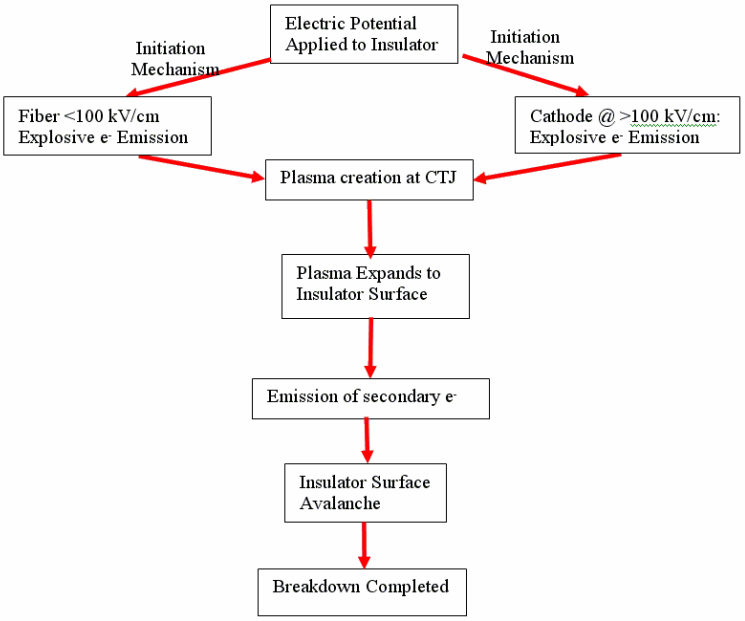

Figure 3: Proposed mechanism for insulator flashover originating from the cathode or cathode triple junction.

Anode Initiated Surface Breakdown:

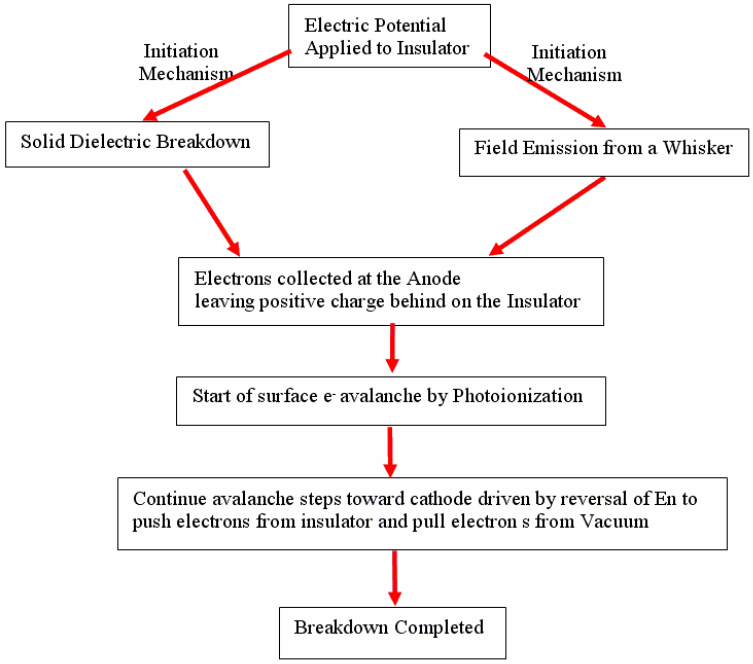

Figure 4: Proposed mechanism for insulator flashover originating from the anode triple junction.

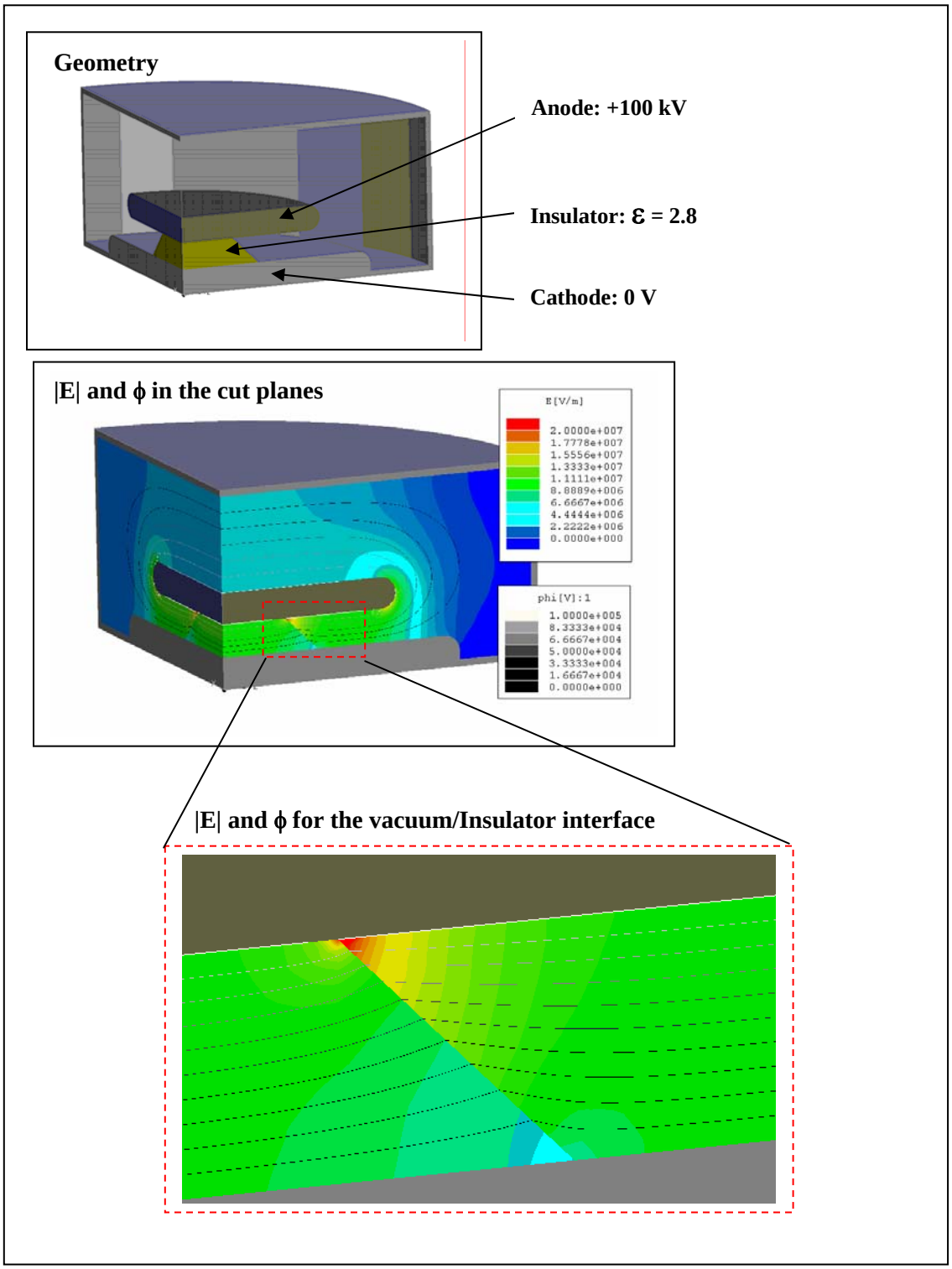

Figure 5: Shows the electric field, |E| in V/m and the equipotentials, ϕ for the base case with Maxwell 3D electrostatic solver. For presentation purposes, and computational economy only ¼ section of the geometry is modeled.

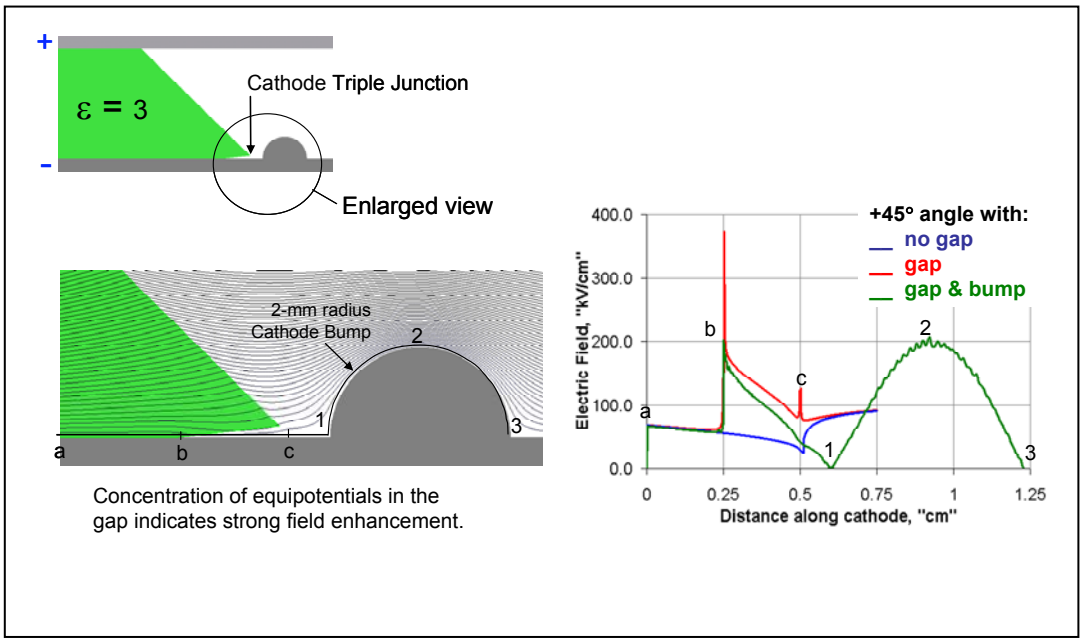

Figure 6: Shows the changes of electric field on the surface of the cathode due to presence of a notch (gap) and a cathode-bump.

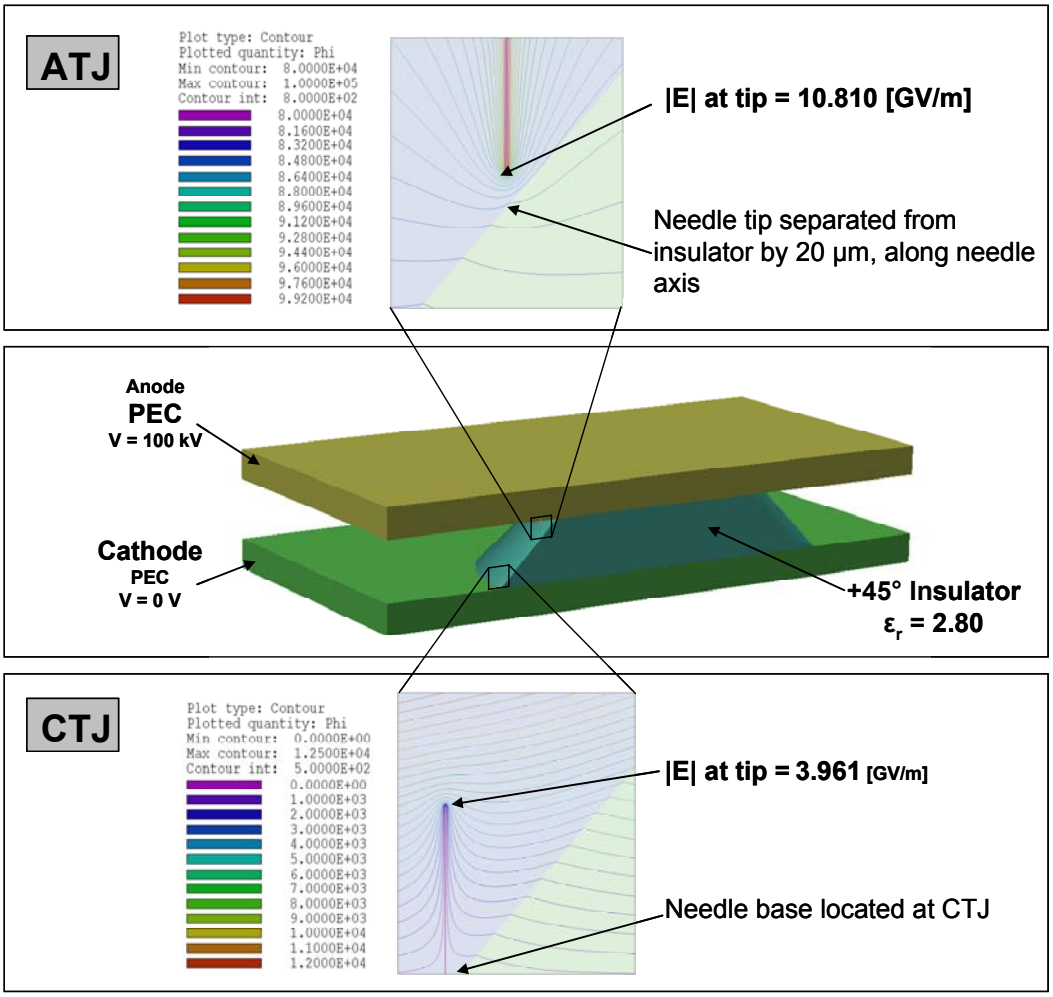

Figure 7: Shows local electric field due to a needle, radius of 1 μm, and length of 1000 μm (micro-protrusion) inserted in at the CTJ and vicinity of ATJ of the 45^0 degree insulator configuration to high level of precision with Trak suite of codes.

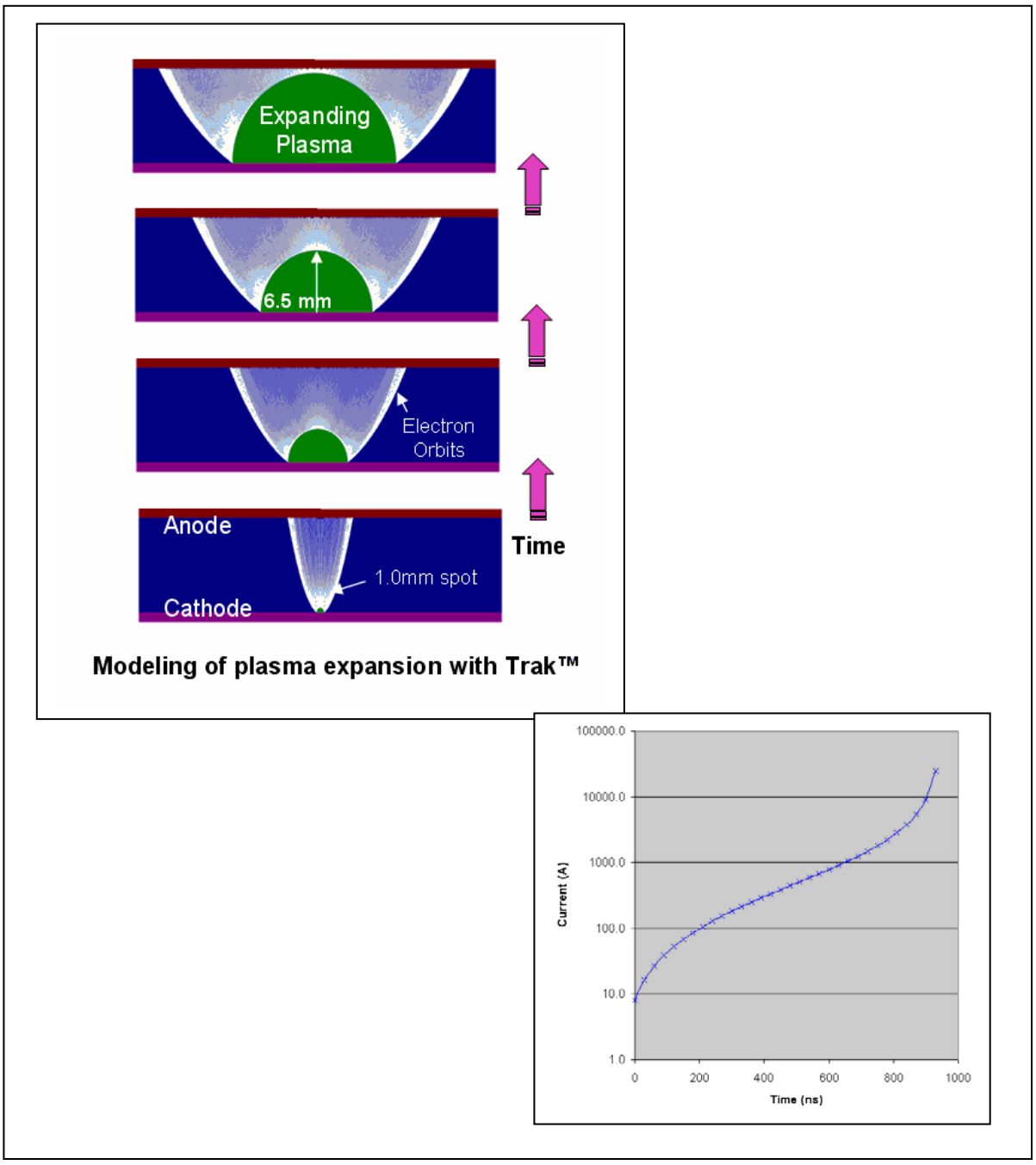

Figure 8: Shows Trak modeling of space-charged-limited electron current from plasma (generated from the velvet-dot) as it expands for different snap shots in time.

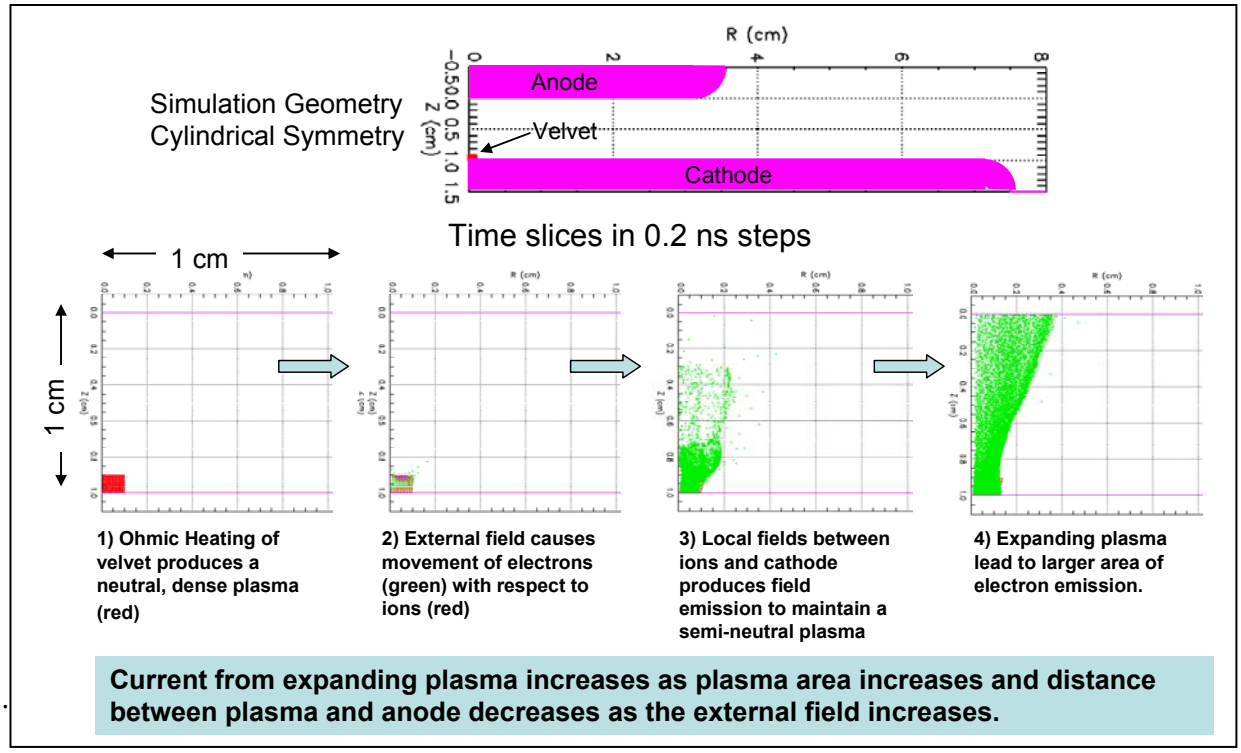

Figure 9: Using LSP to study the initial emission from plasma/velvet.

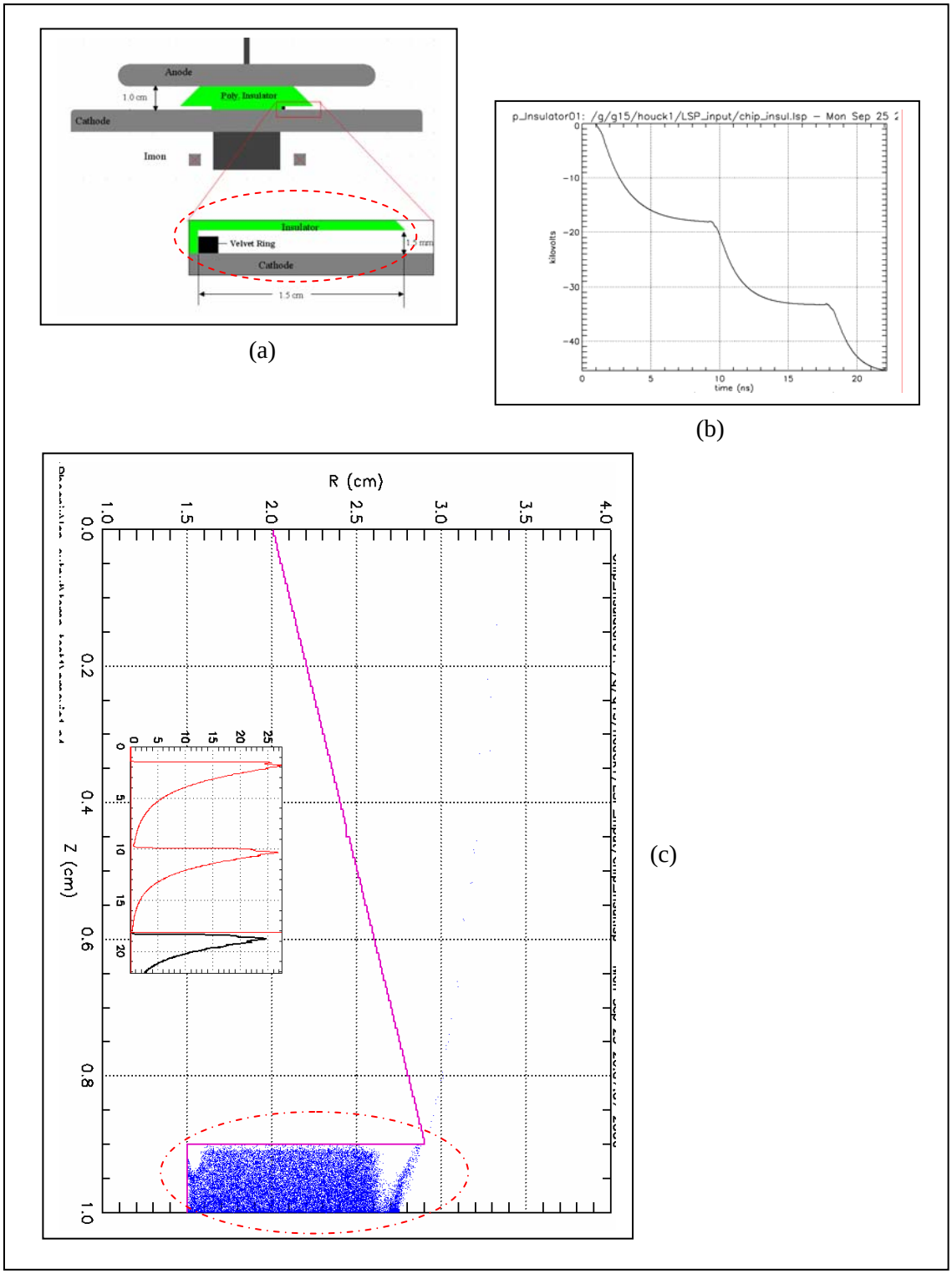

Figure 10: Example of plasma under a radial step in the insulator; (a) a sketch of the geometry, (b) the driving voltage and (c) snap shot in time of plasma emission.

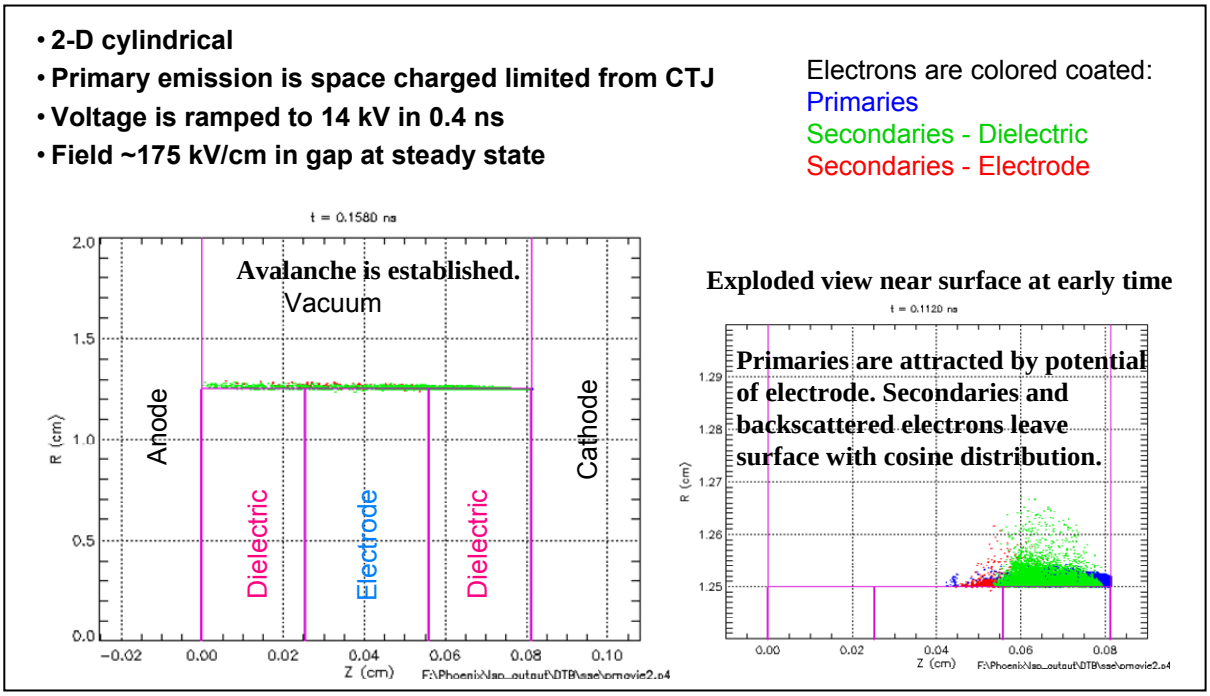

Figure 11: LSP Modeling of Secondary Electron Emission and Electron Avalanche.

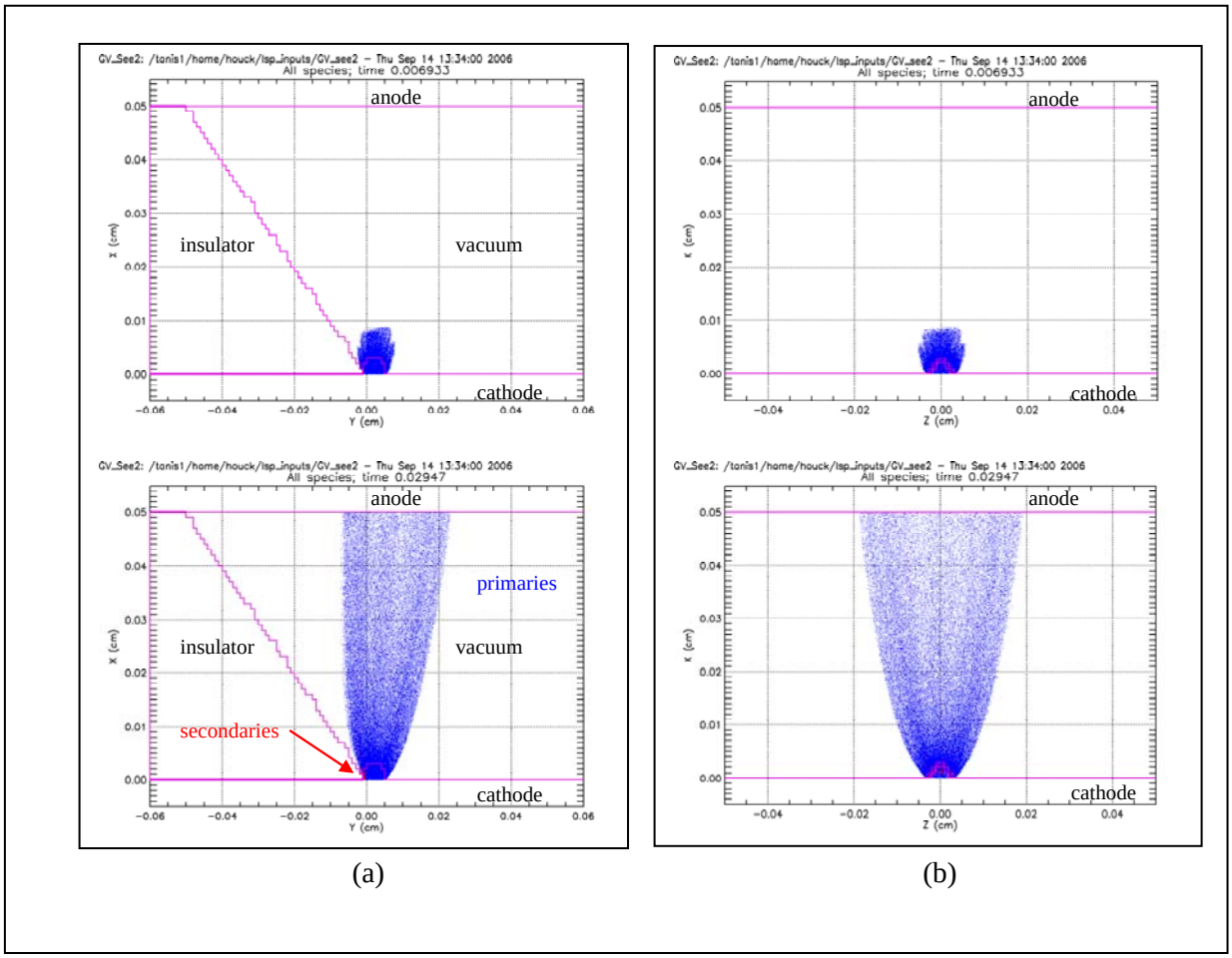

Figure 12: Emission from the CTJ in 3-D: (a) side view and (b) front view.

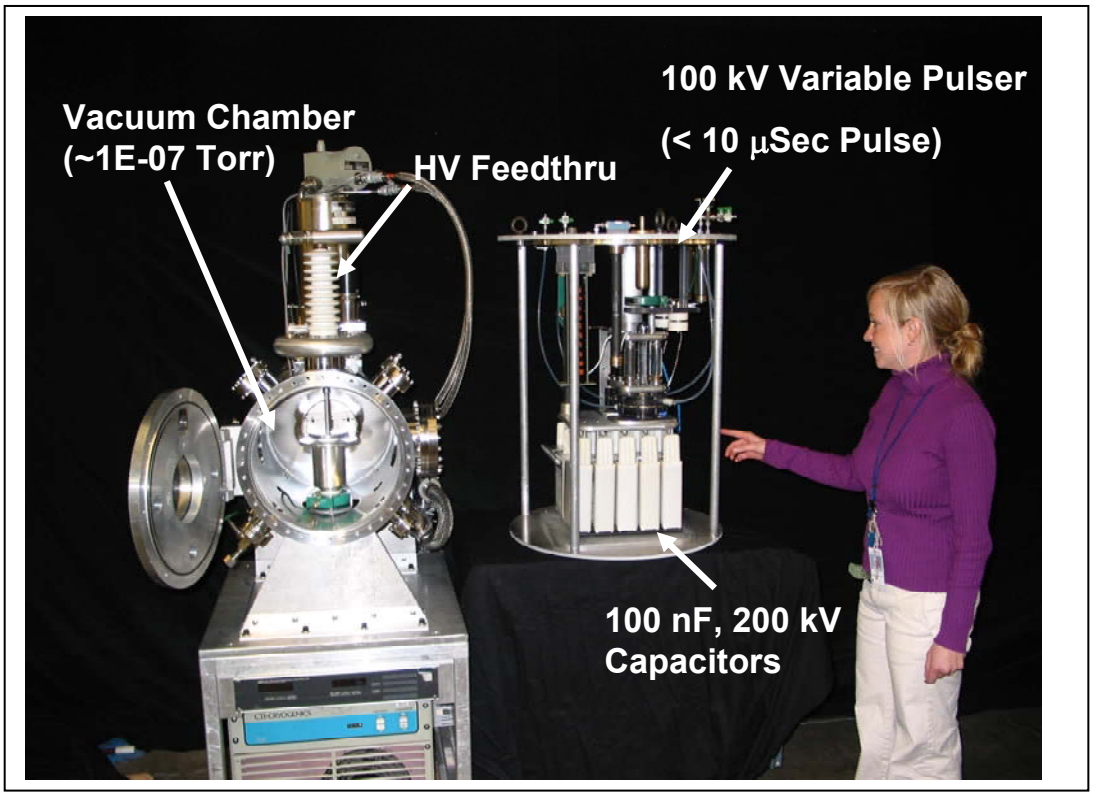

(a)

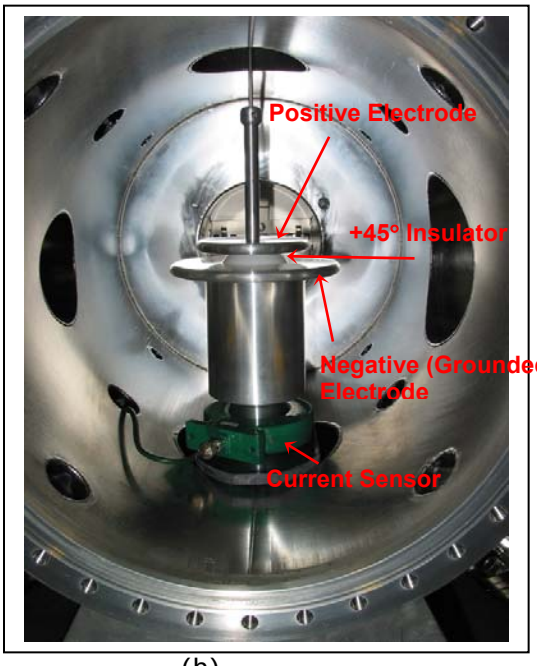

(b)

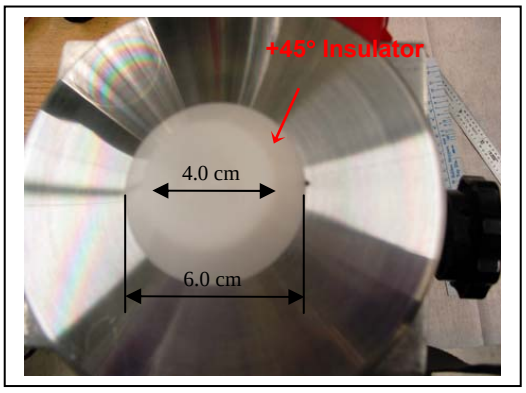

(c)

Figure 13: (a) Photo showing the test stand main components of the vacuum chamber and the pulser, (b) vacuum chamber with a HD polyethylene insulator installed between electrodes, (b) HD polyethylene insulator placement on the cathode.

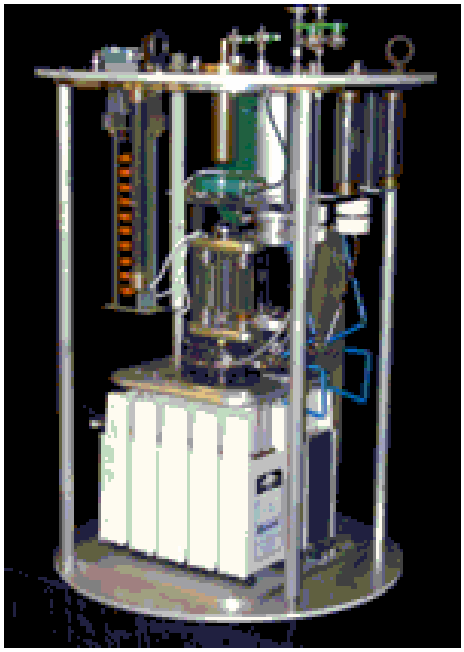

(a)

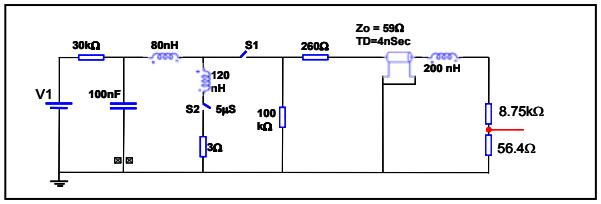

(b)

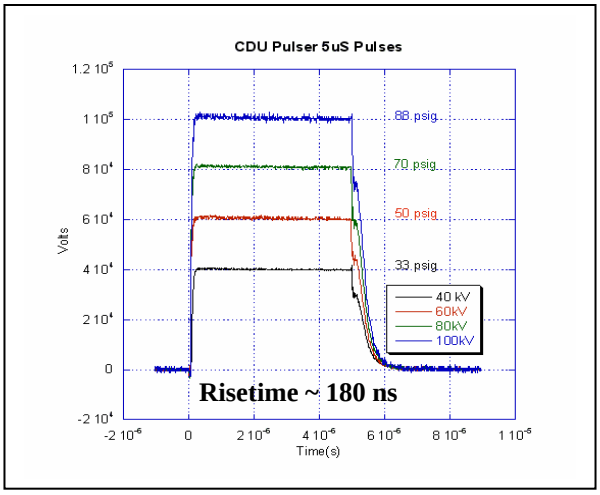

(c)

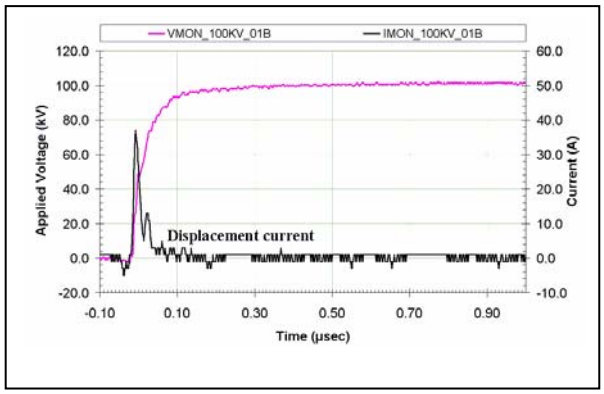

(d)

Figure 14: (a) The compact 100 kV variable CDU about 120 cm in height. The unit is submerged in 55 gal high voltage transformer oil during operation, (b) Circuit diagram of the CDU, (c) The CDU variable applied voltage on a 8.75 kΩ resistive load with 5 μs crowbar time and (d) displacement current for the 100 kV applied voltage.

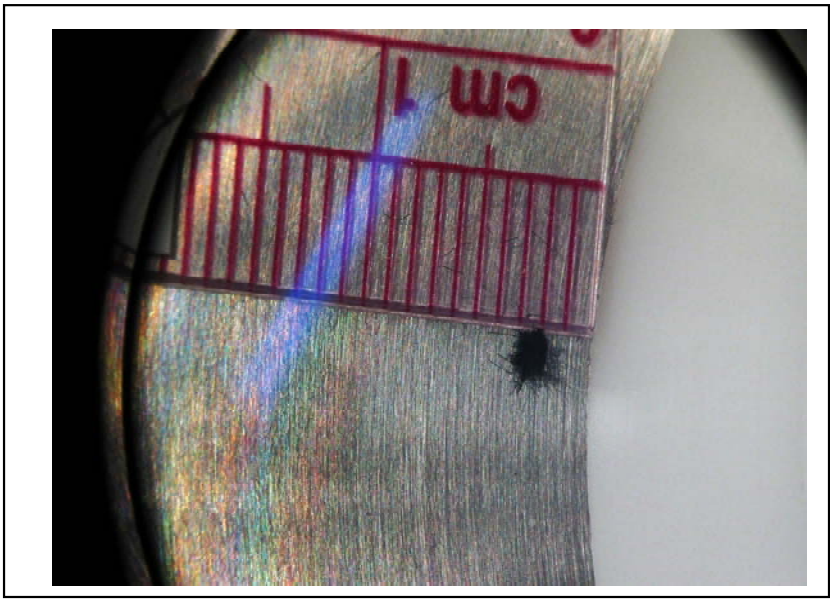

(a)

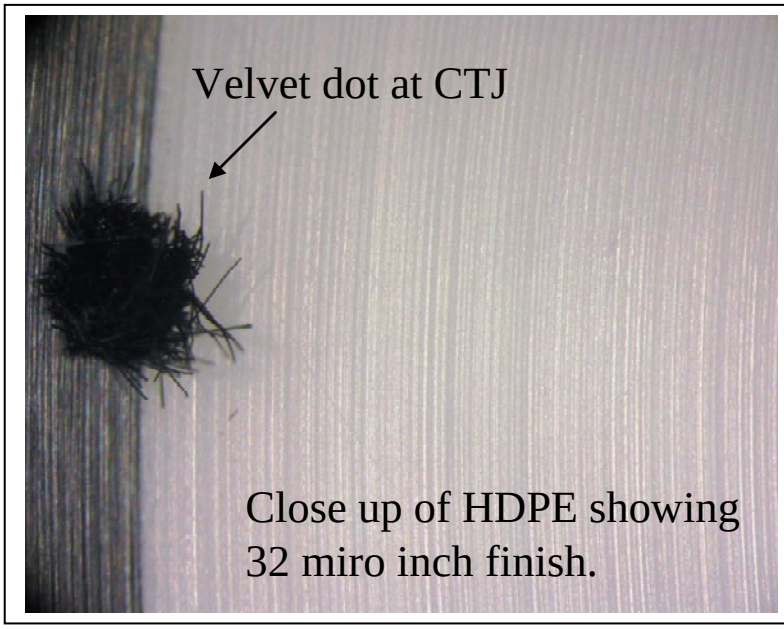

(b)

Figure 15: Photograph of velvet-dot adjacent to insulator.

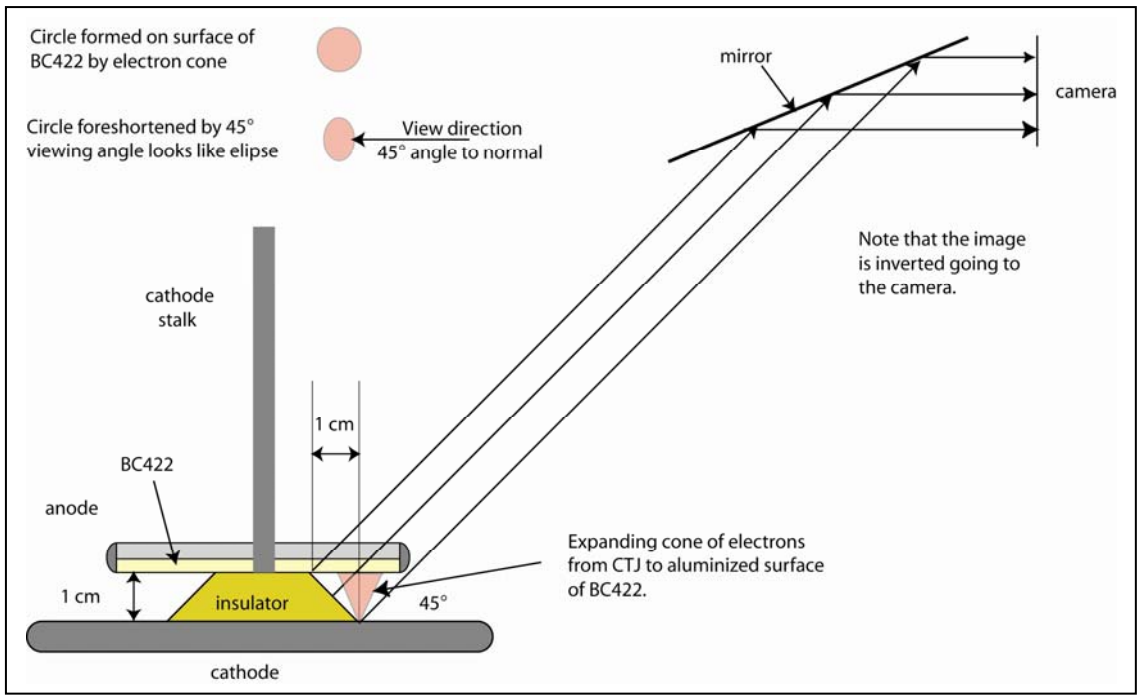

Figure 16: A sketch illustrating the camera viewing angle and a few ray traces from the object back to the camera.

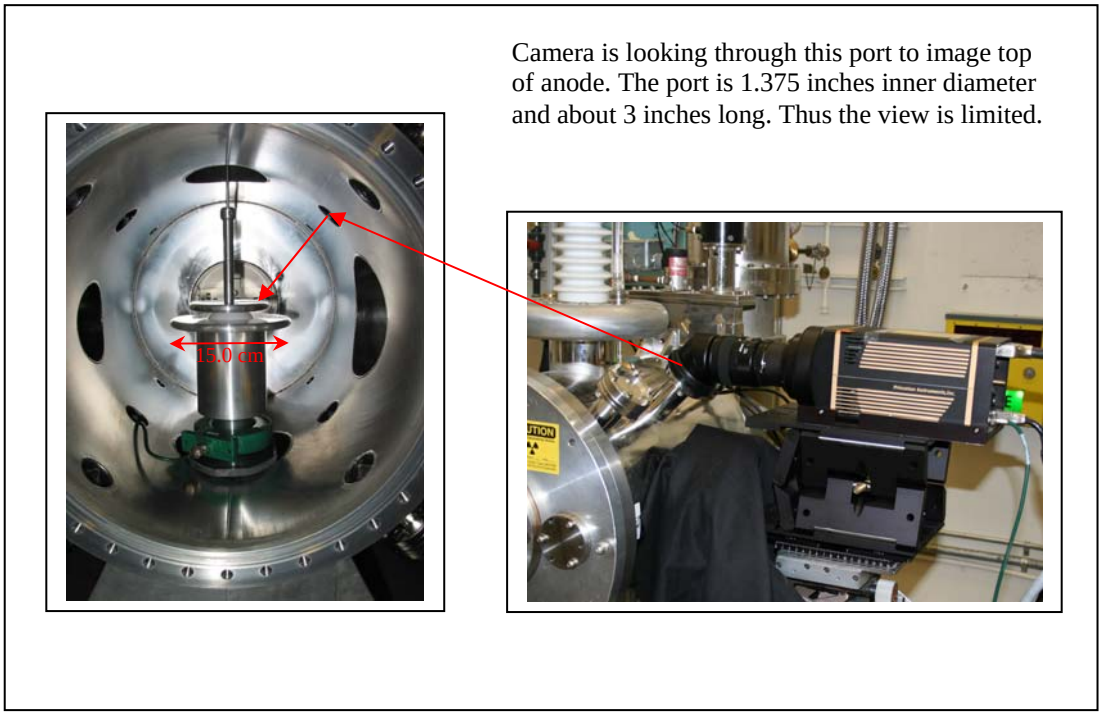

Figure 17: Set up of the PI-Max CCD camera in the actual test stand.

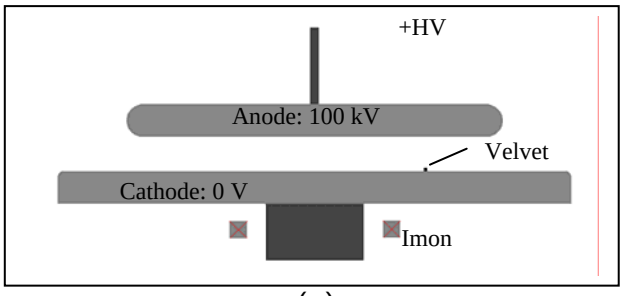

(a)

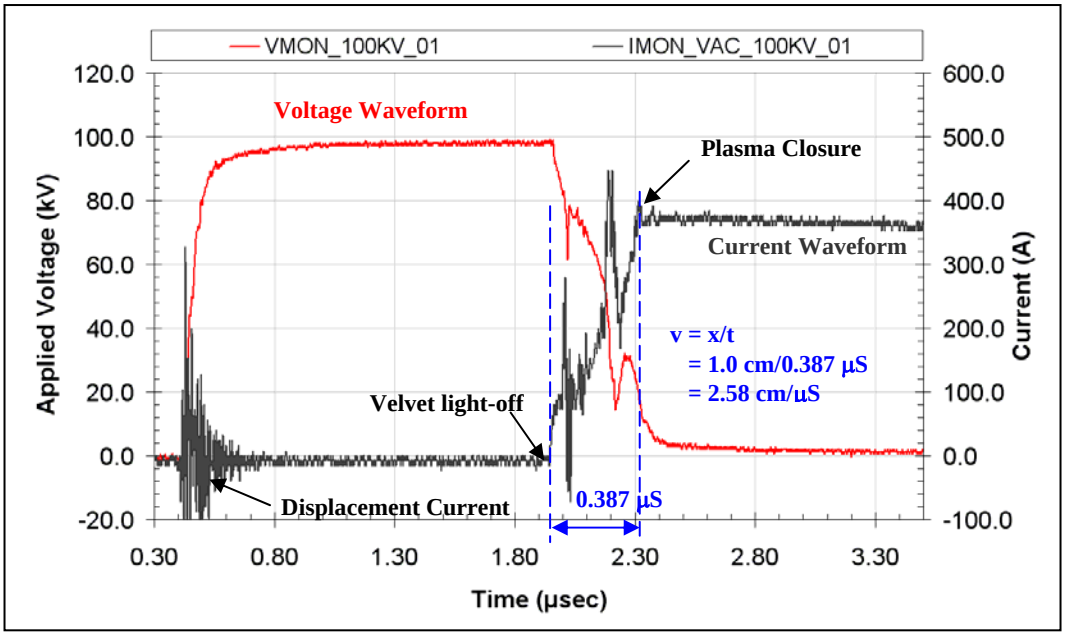

(b)

Figure 18: (a) Test geometry for velvet-dot with no insulator, (b) applied voltage and current waveform for the breakdown of a newly installed tuft of velvet exposed to +100 kV.

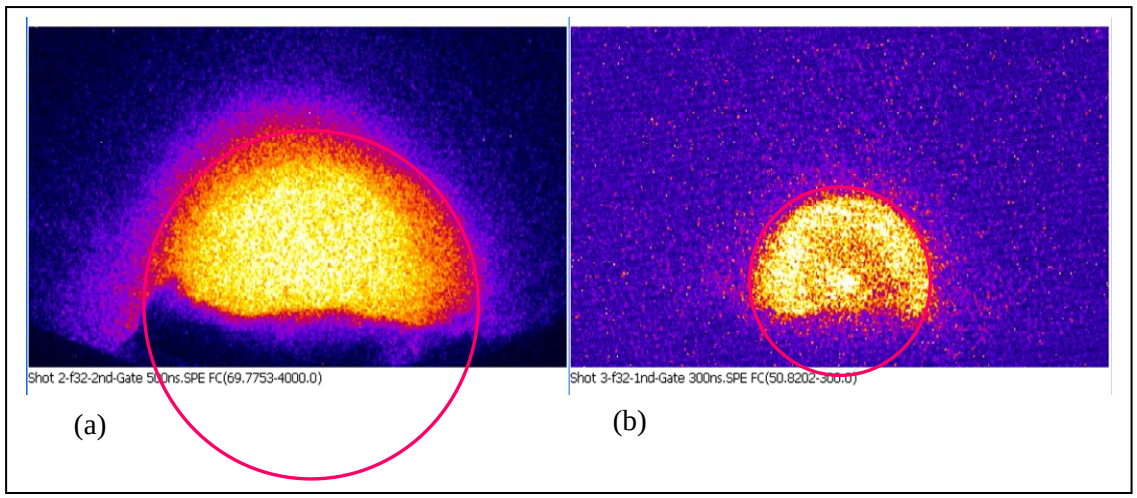

Figure 19: CCD camera false color images of the expanding plasma produced by velvet-dot at two different in times. Expansion cross section is circular; (a) diameter ~ 2.2 cm for gate-width of 500 ns and (b) diameter ~1.4 cm for gate width of 300 ns.

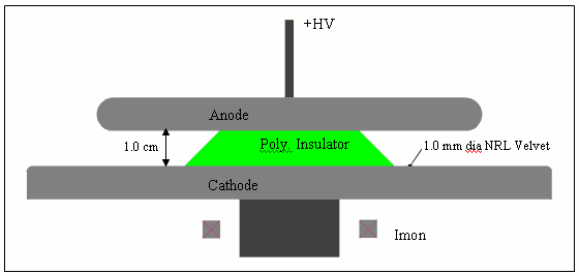

(a)

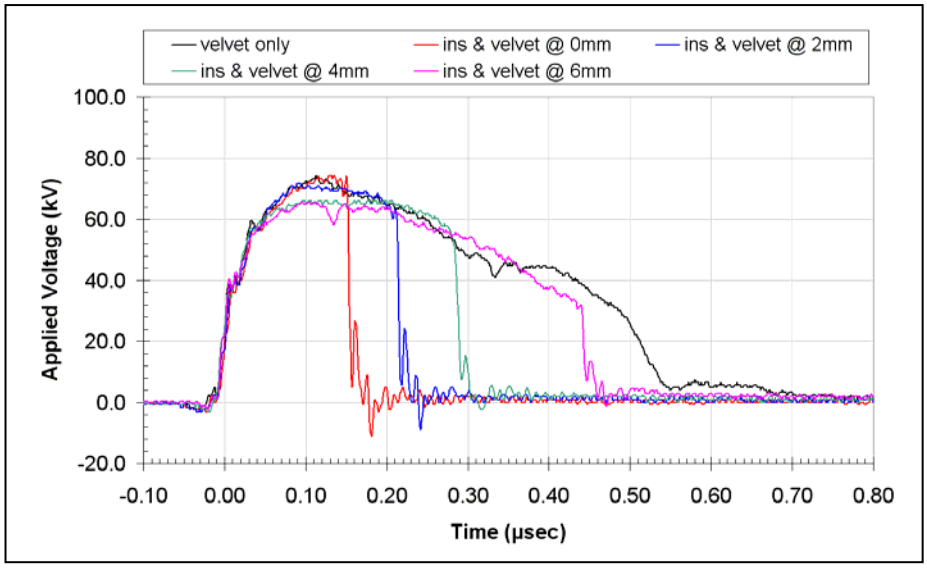

(b)

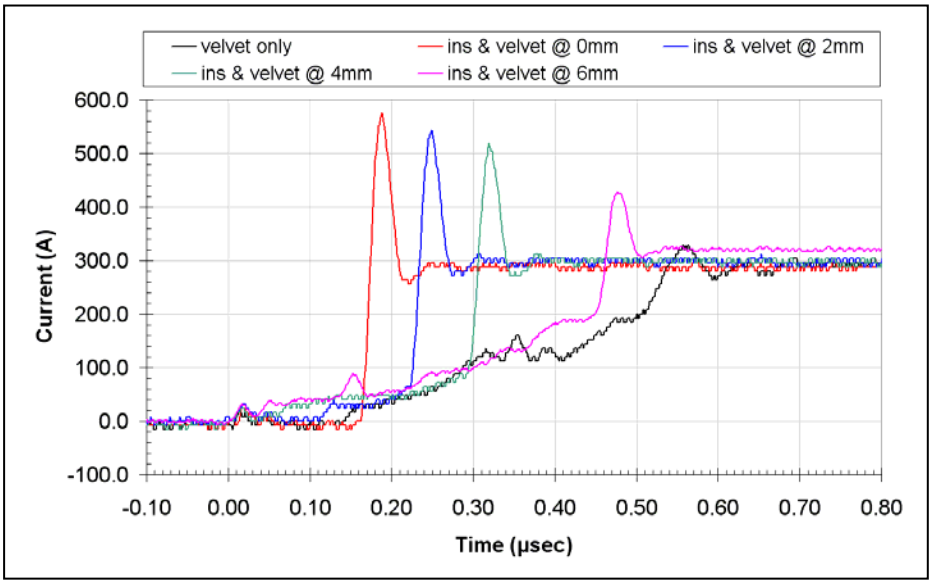

(c)

Figure 20: (a) Test geometry with velvet-dot near the CTJ of +45 polyethylene insulator, (b) Voltage waveform for +80 kV discharge, (c) Current waveform for +80 kV discharge.

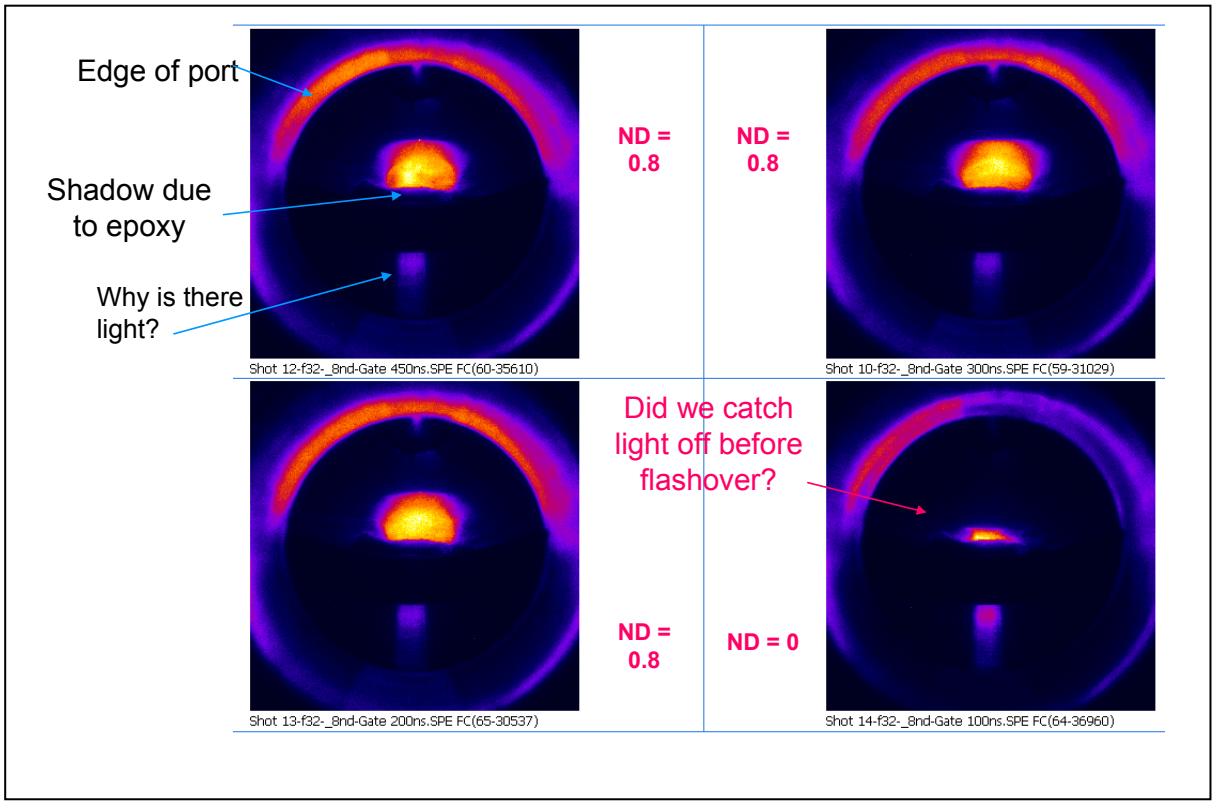

Figure 21: Insulator test with velvet-dot at CTJ. Camera gate width varied slightly while keeping trigger time constant. False color image.

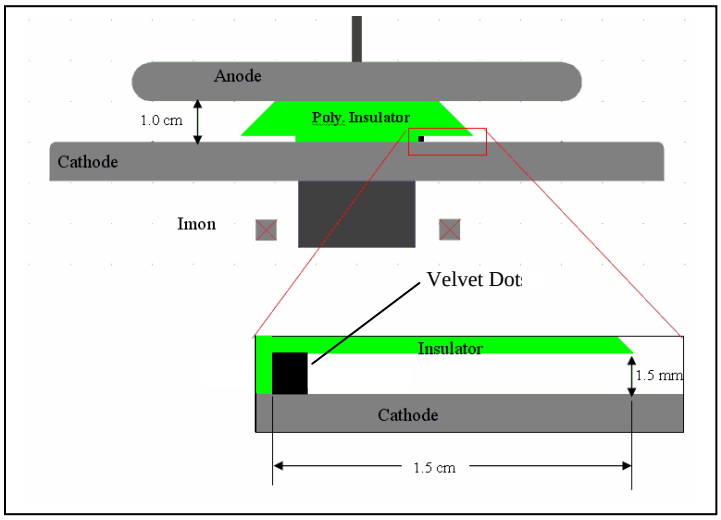

(a)

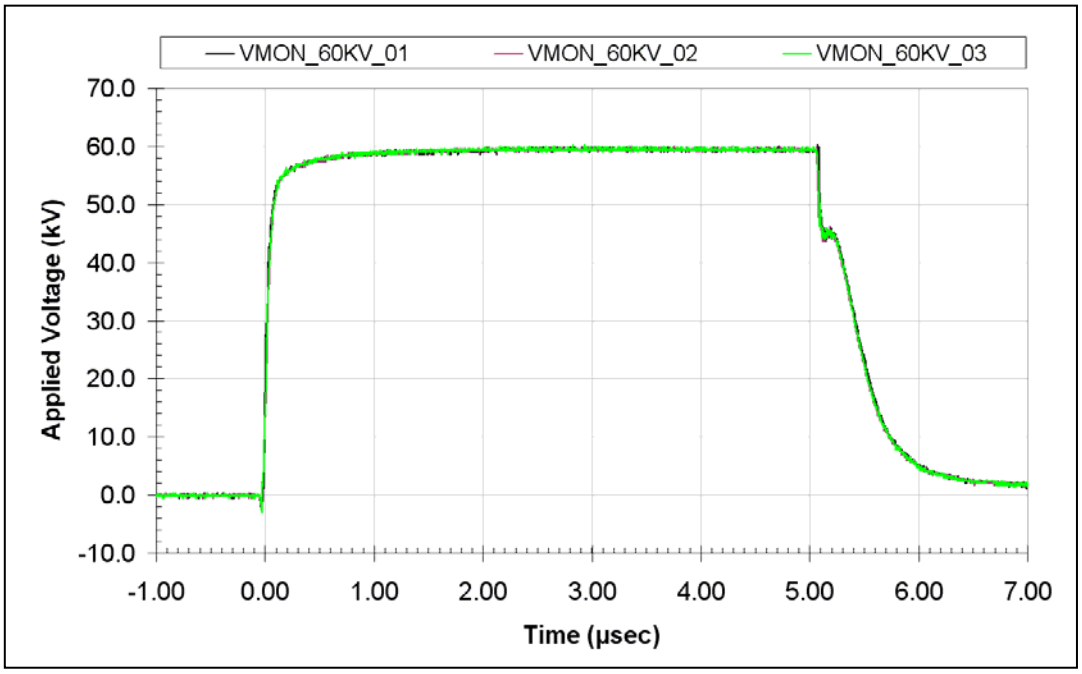

(b)

Figure 22: (a) Test geometry of the radial step underneath the insulator on the cathode side. Test case with velvet-dot installed in the gap. (b) Voltage waveforms for this case at +60 kV. The voltage held consistently for the 3 shots as it did it on previous testing without the velvet-dot.

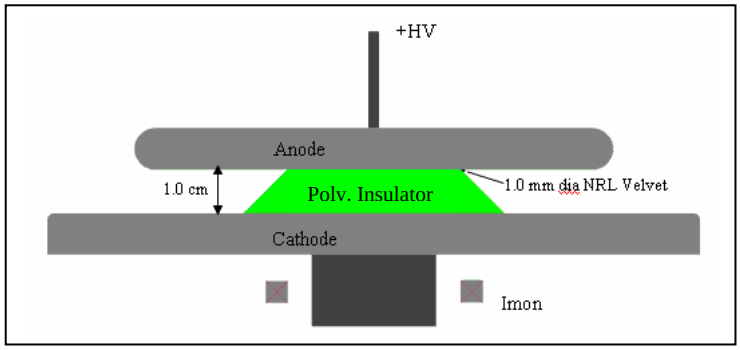

(a)

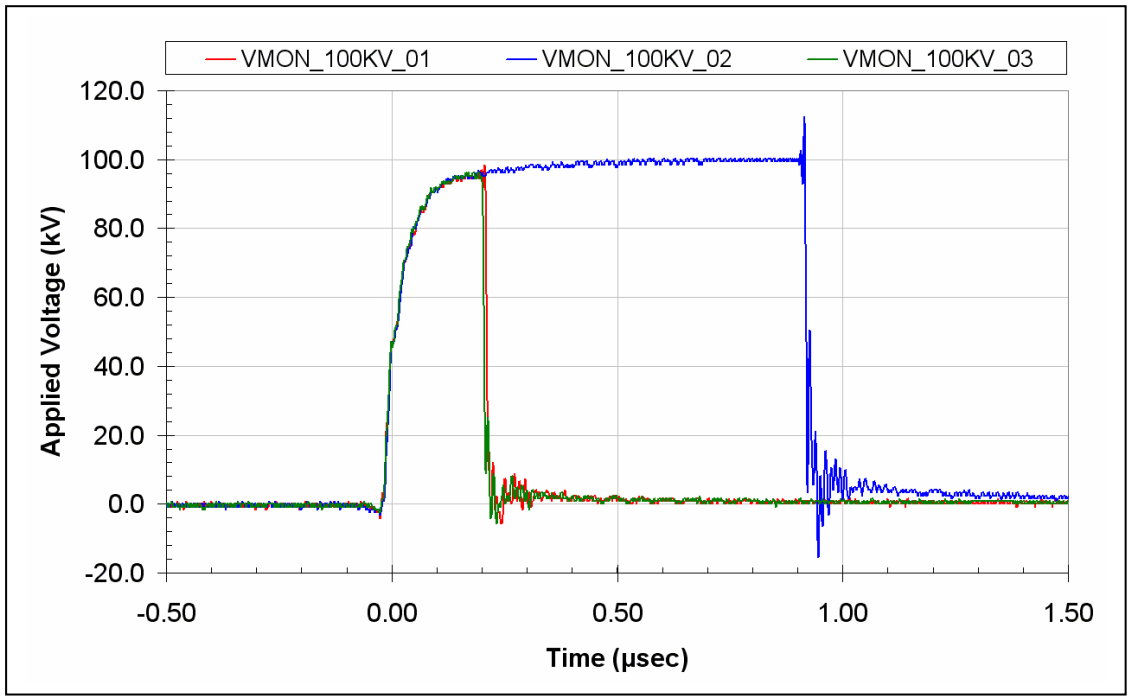

(b)

Figure 23: Test geometry of velvet-dot at the ATJ of Polyethylene insulator and (b) Voltage waveform for +100 kV discharge for 1.0 mm dia. velvet at ATJ configuration.

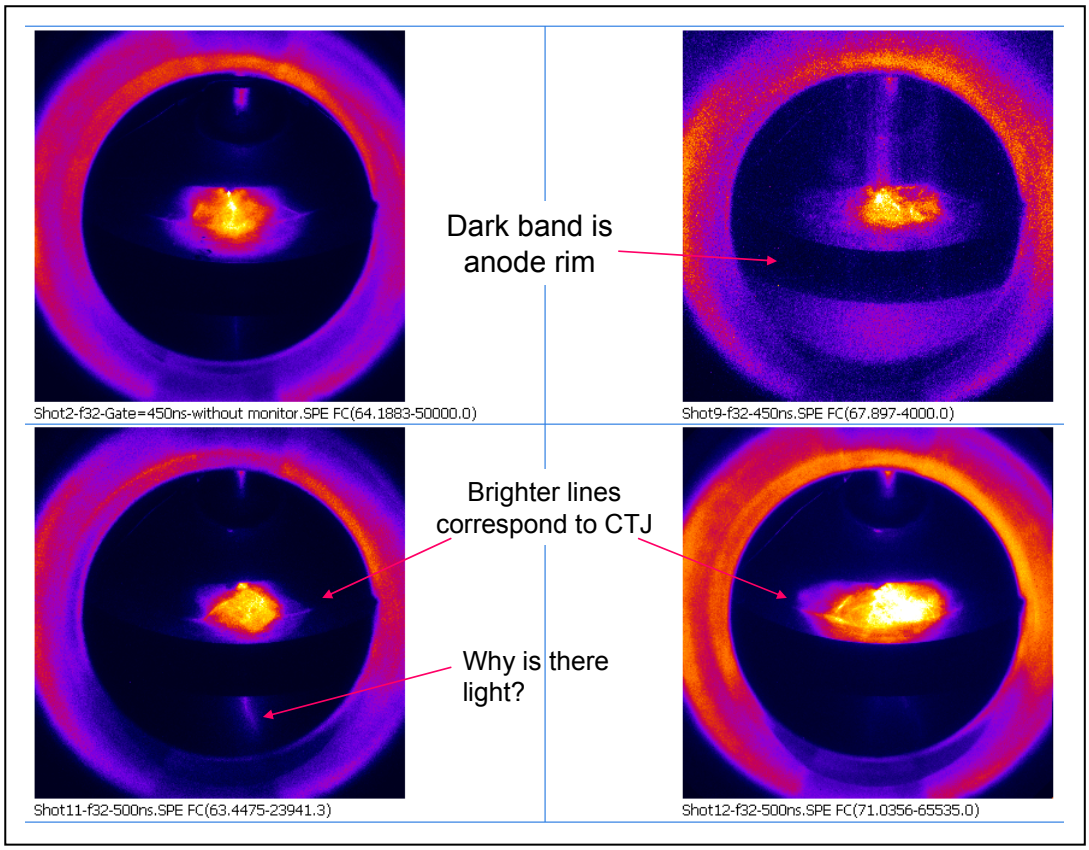

Figure 24: Insulator test with velvet-dot at ATJ shot. Camera gate width varied slightly while keeping trigger time constant. False color.

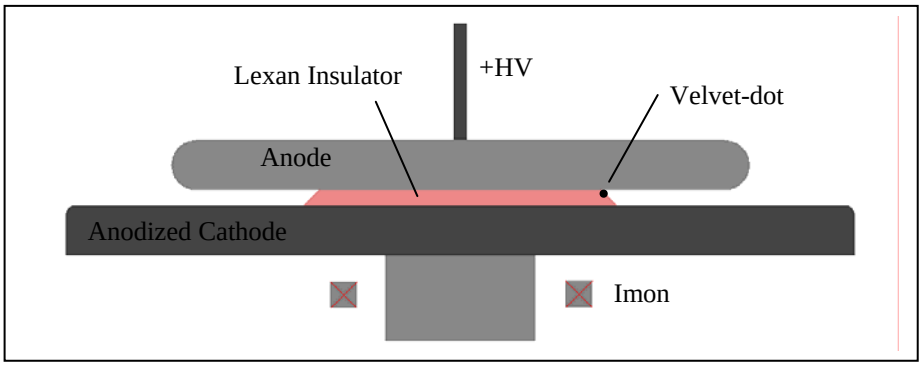

(a)

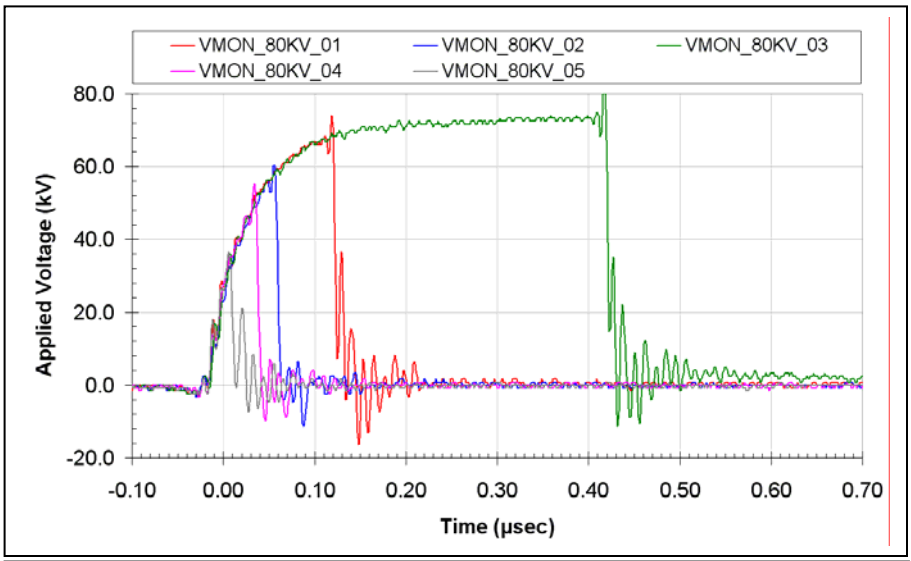

(b)

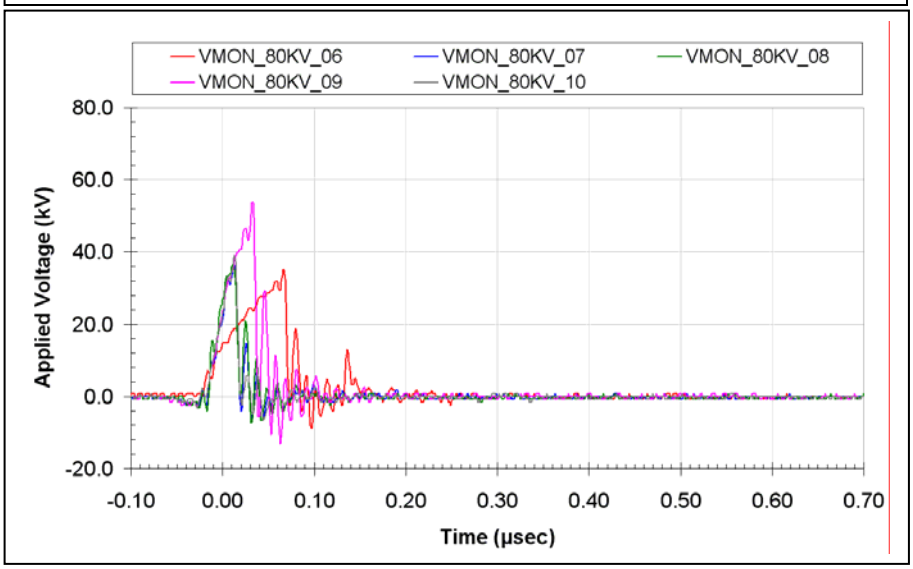

(c)

Figure 25: (a) Test Geometry with velvet at the ATJ of Lexan insulator; 0.3 cm gap. (b) Voltage waveform for Shots 1-5 and (c) Voltage waveform for Shots 6-10.

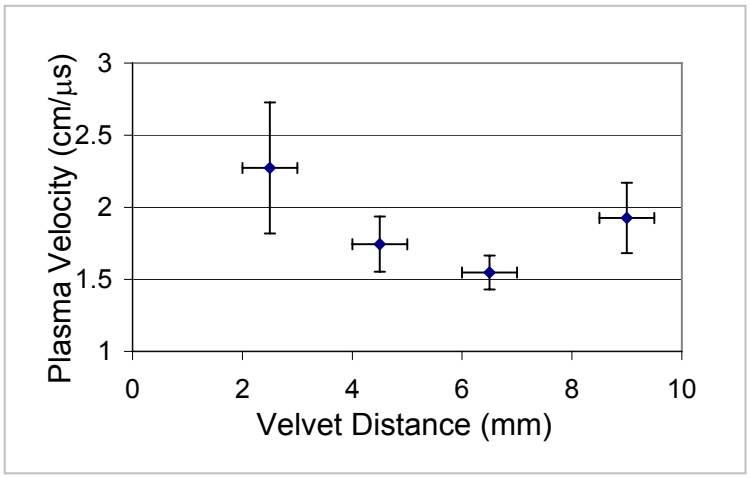

Figure 26: Shows the variation in plasma velocity for various velvet-dot distances away from the cathode. - Error bars indicate uncertainty in location light-off over 1- mm diameter.

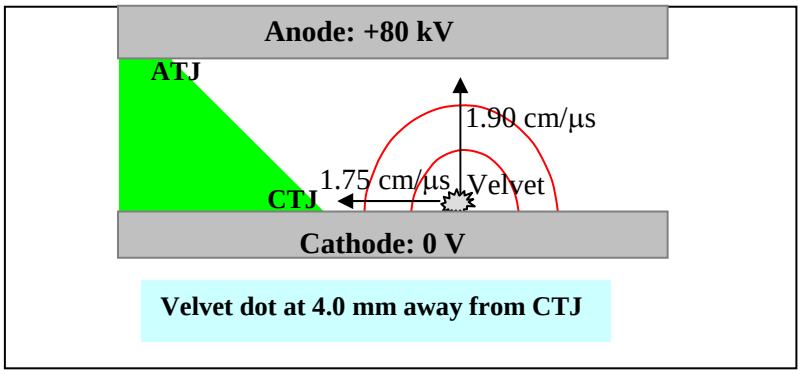

Figure 27: Plasma expansion is not perfectly hemispherical, since it moves faster across the gap than towards the ATJ as shown for the example case of velvet-dot at 4.0 mm away from the CTJ.

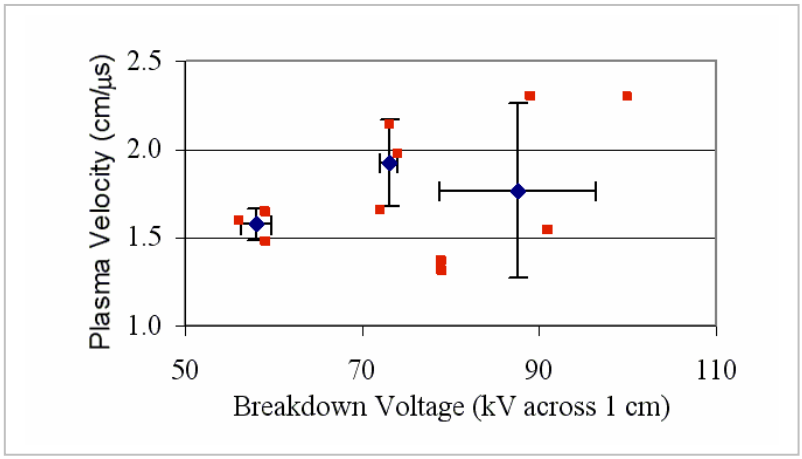

Figure 28: Shows the variation in plasma velocity for various velvet-dot distances as a function of breakdown voltage.

Appendix 1: – The Advantages of Modeling with Trak Code

The Tricomp (two dimensional) and Amaze (three dimensional) suites of finite-element software, or simply referred to as Trak, for electromagnetic solutions including charged particle transport, were originally chosen for the project to model electron and ion emission under steady state conditions. A feature of their electrostatic solvers referred to as the "zoom" feature, has made these codes our primary software for electrostatic simulations. In FEM codes, the maximum resolution attainable for small details within a solution geometry is normally limited solely by the amount of computer memory available. Variable grids can be used to achieve finer resolution for regions of interest, but the computer memory stills limits the maximum number of grid nodes. The zoom option in Trak, essentially allows us to bypass this limitation by dividing the problem over multiple simulations each of which solves for a smaller portion of the original geometry. This is accomplished by using the solution of a previous simulation as a boundary condition for a smaller, contained geometry. Within this smaller geometry, a finer solution grid may be used consisting of no more grid nodes than the larger geometry. Repeated application of the zoom allows almost unlimited resolution.

A few caveats:

1) Details, e.g. bumps, inclusions, whiskers, etc., not resolved in the simulation used for the boundary condition must be located sufficiently far from the boundary in the subsequent simulation that they have negligible effect on the solution at or near the boundary.

2) The zoom concept is not new. Simulators have been using boundary conditions based on symmetry arguments, analytical solutions, and other simulations to limit the extent of simulations for many decades. What makes the Tricomp and Amaze software unique is the flexibility, accuracy, and integration of the concept in the software. The drawback is that it is inefficient requiring multiple simulations to achieve high resolution.

3) An alternative to the zoom used in software such as Maxwell and FlexPDE is the variable, conformal grid. This approach allows a fine grid (high resolution) in regions of rapidly changing fields and small details while regions of slower change use a much coarser grid. This approach is faster, much more efficient, and normally provides sufficient resolution. The drawback is that it is very difficult or impossible to achieve higher resolution than provided by the default code settings. Typically, we use a variable, conformal grid code first to see if it is sufficient, and use the Tricomp and Amaze software only if higher resolution is needed.

Appendix 2: – Micro-protrusion (Dielectric Fiber) Modeling

A dielectric fiber (velvet fiber), at the CTJ in a high voltage vacuum insulator test apparatus can act as an electron source, and force the onset of dielectric breakdown. Electrostatically, we have modeled a micro-protrusion, in the shape of a needle, inserted at the CTJ and ATJ of a 45 degree insulator.

The geometry that is modeled is shown in Figure A2.1. The geometry shown is a half-geometry; the complete geometry has been bisected along the micro-protrusion for visibility purposes.

Electrostatic modeling was performed using Field Precision's AMAZE software suite. This software package was selected due to its ability to model details whose physical dimensions are orders of magnitude smaller than the global solution space. This process is performed by extracting potentials along six 2D planes of a solution that contain a smaller space, and applying those potentials to the boundaries of the smaller, contained space as a new solution volume.

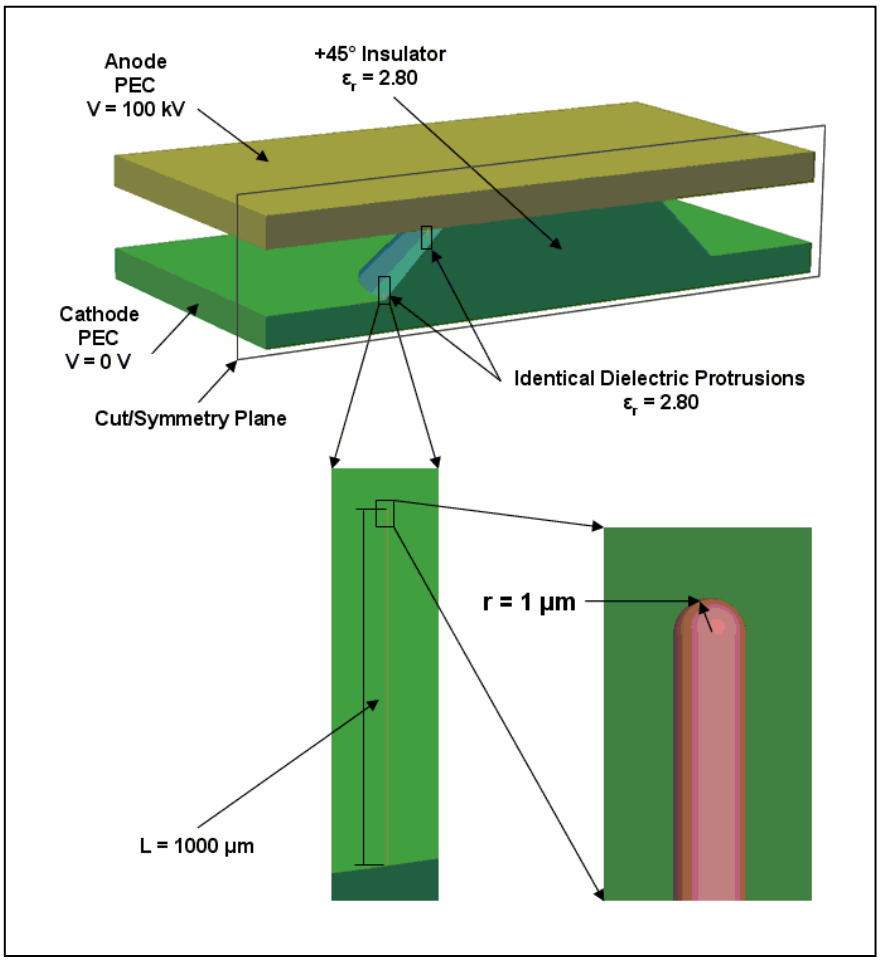

Figure A2-1: Modeled geometry for micro-protrusion (dielectric fiber) effect.
The velvet fiber is modeled as a cylindrical shaft, with radius 1 µm, which is capped by a hemispherical tip, of radius 1 µm. The length of the needle, from its base on the cathode to its tip, is 1000 µm. The dielectric constant used for the velvet was 2.80.The separation between the planar anode and cathode is 1 cm.
One fiber is placed at CTJ and one fiber is placed in the vicinity of the ATJ.

Plots for potential and |E| are shown in Figure A2-2 for the needle in the vicinity of the CTJ. Some degree of polarization in the dielectric needle is made evident by the slight depression of field within the needle (not obvious in the above plots), and the enhancement of the field at the tip.

The magnitude of the field inside the needle are roughly 50 times that provided by [1]. According to [1] cathode plasma is formed via surface flashover along the length of the velvet fibers when the electric field exceeds 16 kV/cm.

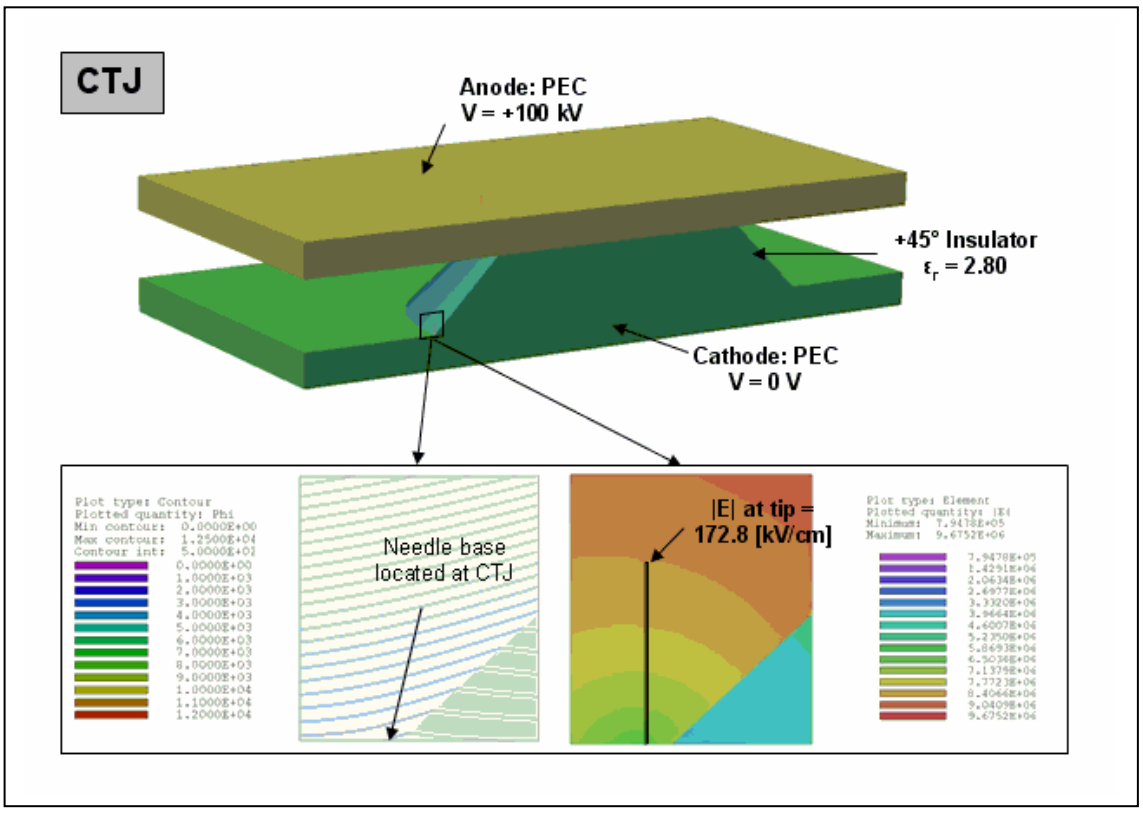

Figure A2-2: Equipotentials and |E| for dielectric fiber at CTJ.

[1] R. B. Miller, J. Appl. Phys. 84, 3880 (1998)

Plots for potential and |E| are shown above for the needle in the vicinity of the ATJ. Some degree of polarization in the dielectric needle is made evident by the slight depression of field within the needle (not obvious in the above plots), and the enhancement of the field at the tip. See Figure A2-3.

An examination of the field distribution at the tip of the dielectric needle will be investigated more closely on a following page.

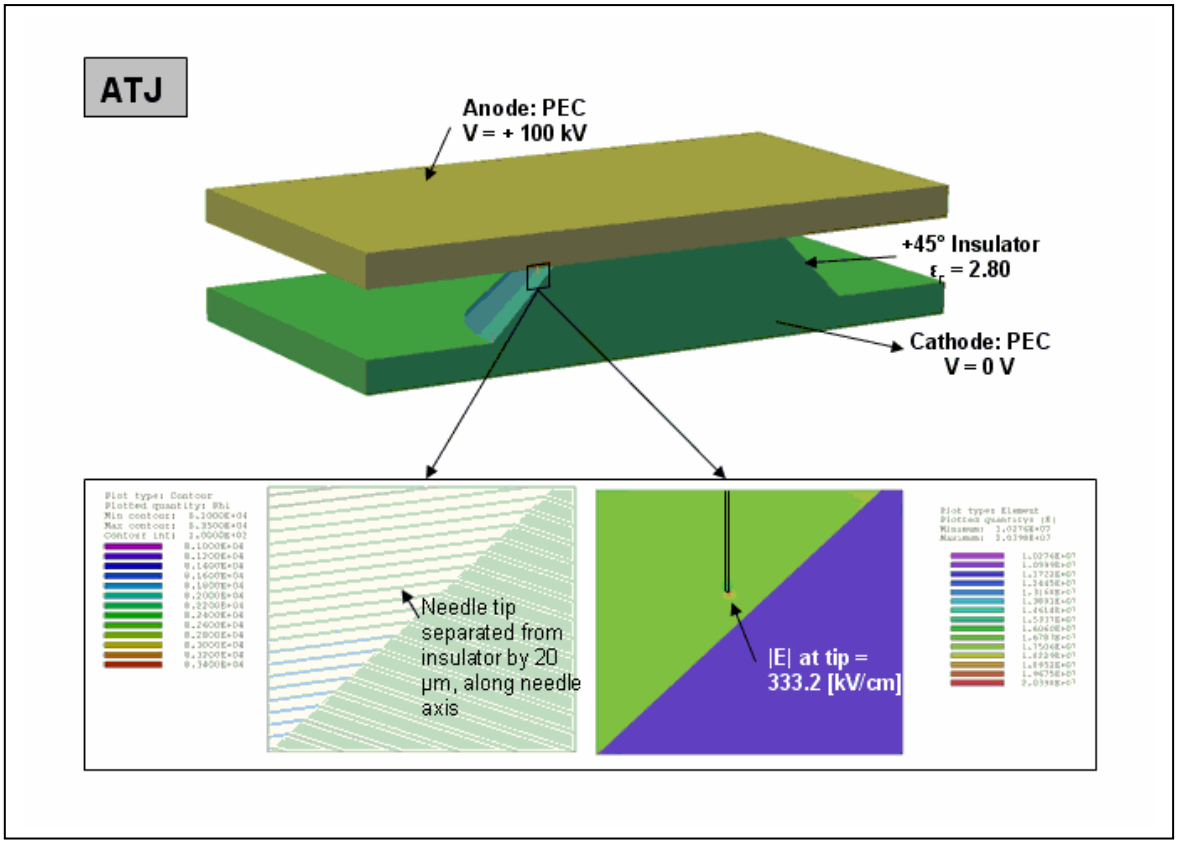

Figure A2-3: Equipotentials and |E| for dielectric fiber at ATJ.

Near the tip of the anode-region needle, the peak |E| field occurs slightly towards the insulator (grey arrow); on the cathode-region needle, the |E| field is slightly depressed towards the insulator (pink arrow). Both plots use the same scale, located above. The units for are [V/m].

The mesh is formed with approximately cubic hexahedra with edges that are roughly 36 nanometers in length.

Note: Experimentally, we have seen surface breakdown of the velvet fiber in the presence of the insulator when a velvet-dot of 1.0-mm was placed at CTJ and then ATJ. The plasma formation for the fibers at the CTJ is a to be expected.

The breakdown that is observed with ATJ is highly suspected that is not due to plasma formation but due to a different mechanism – explained in section II.A.5.of the text. In the case of velvet at the ATJ, some of the fibers are in contact with the insulator. The polarization on the velvet tip in this case has a small shift toward insulator, meaning that the polarization can draw charge from the insulator effecting the reversing the E_{norm} component of the field to the degree to start a surface avalanche in accordance to the theory put forth by E.J. Lauer. Although, we have not done this test at the writing of this report; we speculate that a velvet-dot without the insulator would not emit plasma.

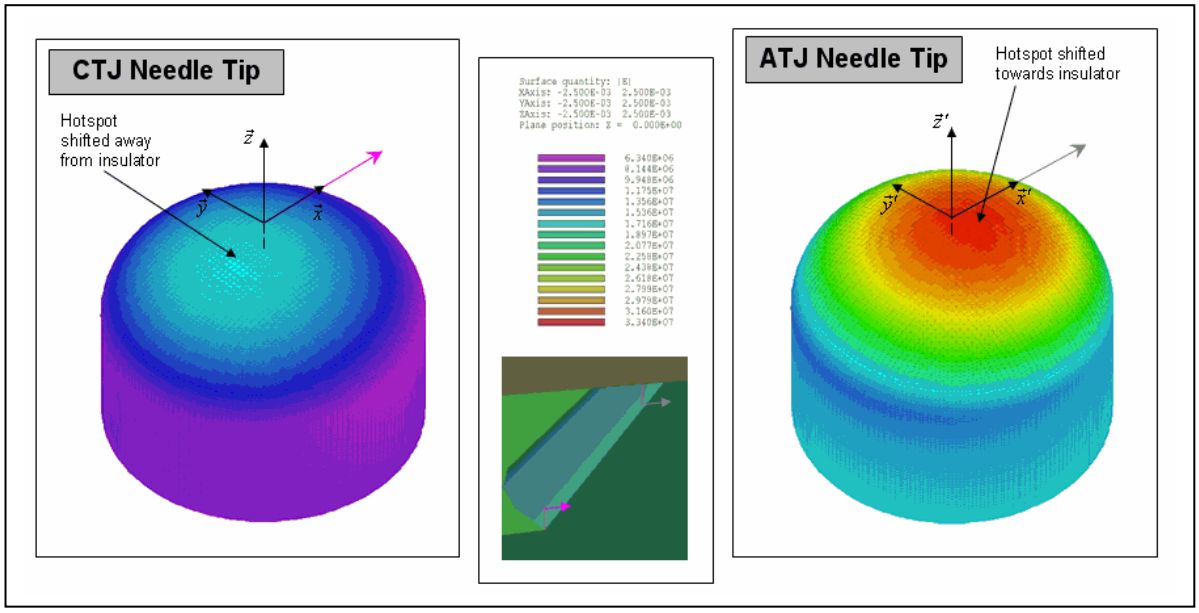

Figure A2-4: |E| plot for the tip of the fibers at CTJ and ATJ.

Appendix 3: – Trak Field Modeling of ATJ and CTJ to High Resolution

Below is the example case where zoom was used in order to study the electric field in the triple junctions; electric field at the vacuum interface of the +45^{o} insulator was analyzed for two cases of 1) 30 μm mesh and 2) 0.2 μm mesh. It turns out that the electric field values at the triple junctions depends on the mesh size. Finer mesh gives higher filed values at the ATJ and lower filed values at the CTJ. This is in agreement with an analytical formulation postulated by Chung et. al. [1] as illustrated in the following pages:

Case study in Trak:

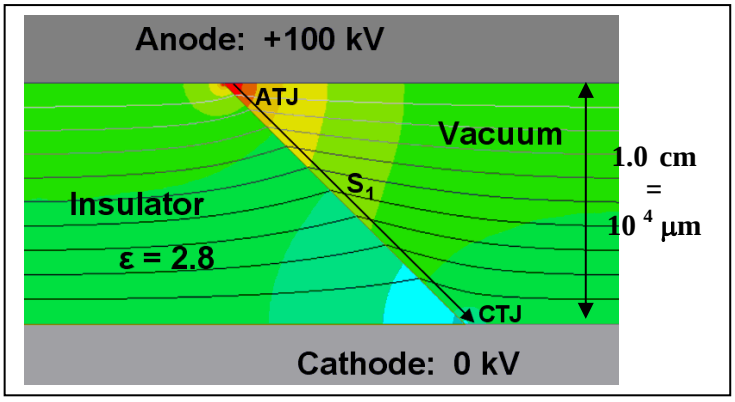

Planar Geometry, |E| and ϕ lines for an Applied Field of +100 kV. Mesh Size: 30 μm.
The line S1 is on the vacuum side, at a distance of 30 μm (1 mesh) away from interface. S1 Starts at the ATJ and finishes at CTJ.

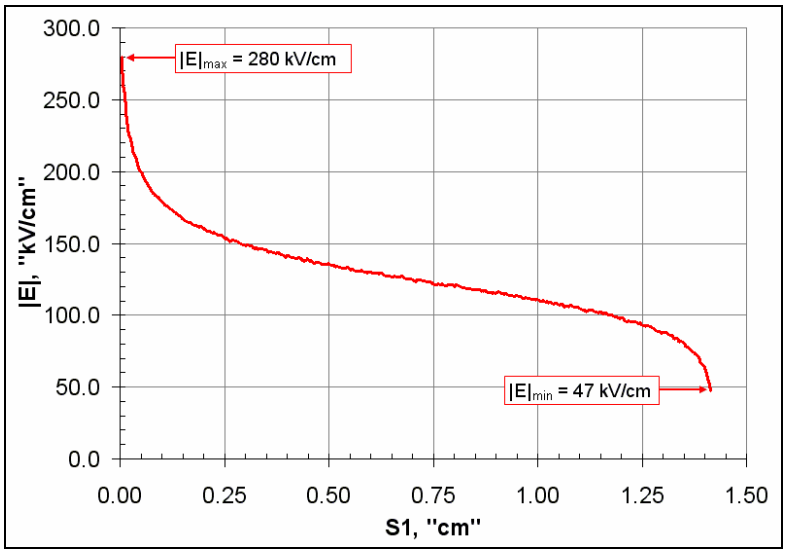

30 μm mesh: Variation of |E| along S_1.
$|E|_{max} = |E|_{ATJ} = 280$ kV/cm and $|E|_{min} = |E|_{CTJ} = 47$ kV/c

M.S. Chang, B-G. Yooh, P.H. Cutter, N. M. Mickowski, J. Vac Sci. Tech, 6 22 1240 (2004)

Trak's zoom feature is used on ATJ and CTJ for 0.2 μm mesh.

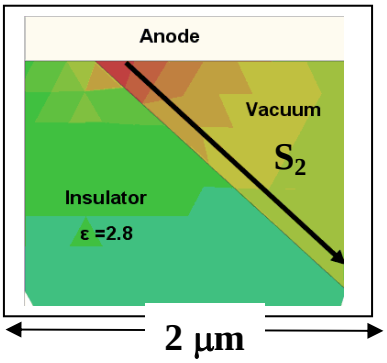

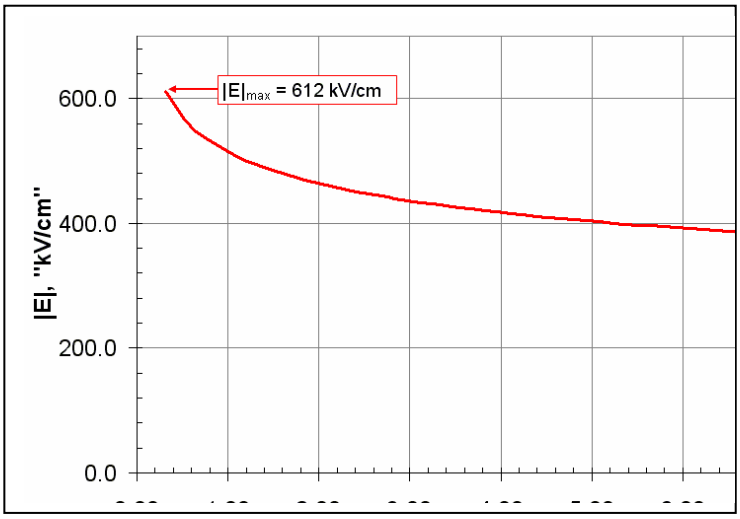

0.2 μm mesh: Variation of |E| along S_2
$|E|_{max} = |E|_{ATJ} = 612$ kV/cm

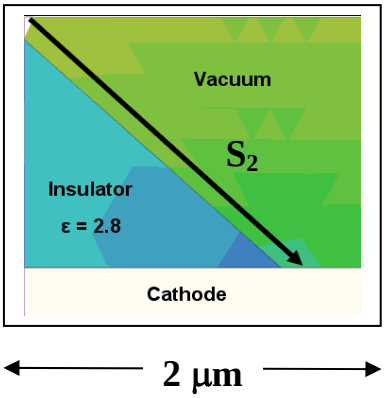

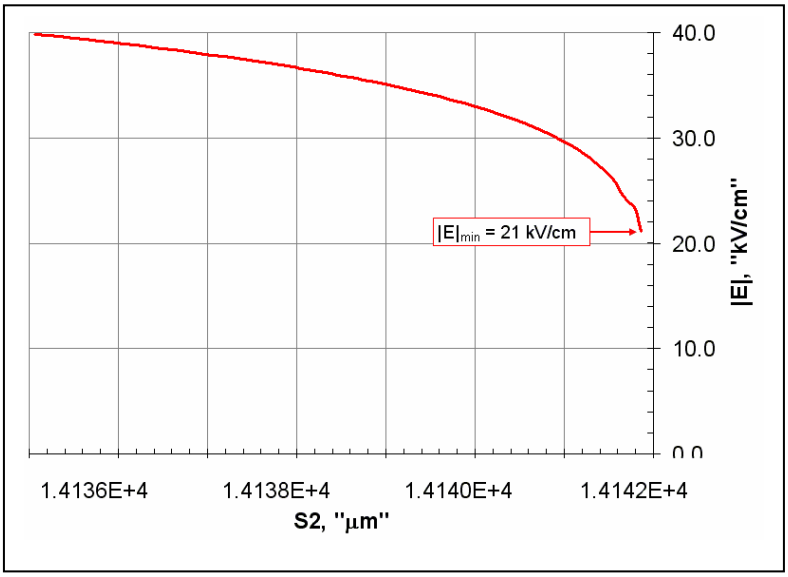

0.2 μm mesh: Variation of |E| along S_2
$|E|_{min} = |E|_{CTJ} = 21$ kV/cm

Mesh Size, μm	$\|E\|_{ATJ}$, kV/cm	$\|E\|_{CTJ}$, kV/cm
30.0	280	47
0.2	612	21

Analytically Chung et. al, have shown that electric field and potential at the triple points of an angled insulator is in the form of:

$$E = Ar^{\nu-1} \quad \text{and} \quad \Phi = Br^{\nu}\sin\nu\left(2\pi-\alpha-\phi\right)$$

Where, r is the distance away from ATJ or CTJ, and A is a function of applied voltage, system geometry, and ε. The claim is:

$$\begin{cases} r \to 0; & E_{ATJ} \to \infty \\ r \to 0; & E_{CTJ} \to 0 \end{cases}$$

An upper bound for r is not given – but can be deduced computationally!

For ATJ, ν is determined from transcendal equation: $\varepsilon\tan\left(\nu\theta\right) = \tan\left(\pi-\nu\beta\right)$

Where the angles are given:

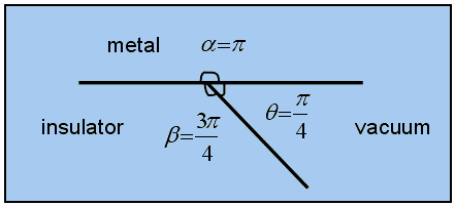

For CTJ, ν is determined from transcendal equation: $\varepsilon\tan\left(\nu\theta\right) = \tan\left(\pi-\nu\beta\right)$

Where the angles are given;

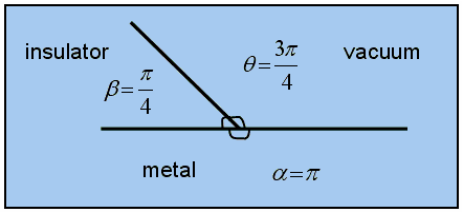

For our +45° insulator geometry,

$$\begin{cases} \nu_{ATJ} = 0.84778 & \to E_{ATJ} = Ar^{-0.15222} \\ \nu_{CTJ} = 1.15222 & \to E_{CTJ} = Ar^{+0.15222} \end{cases}$$

The question of how close the above formulation fits the Trak data for the 30 μm and 0.2 μm is investigated next:

1) 30 μm mesh case:

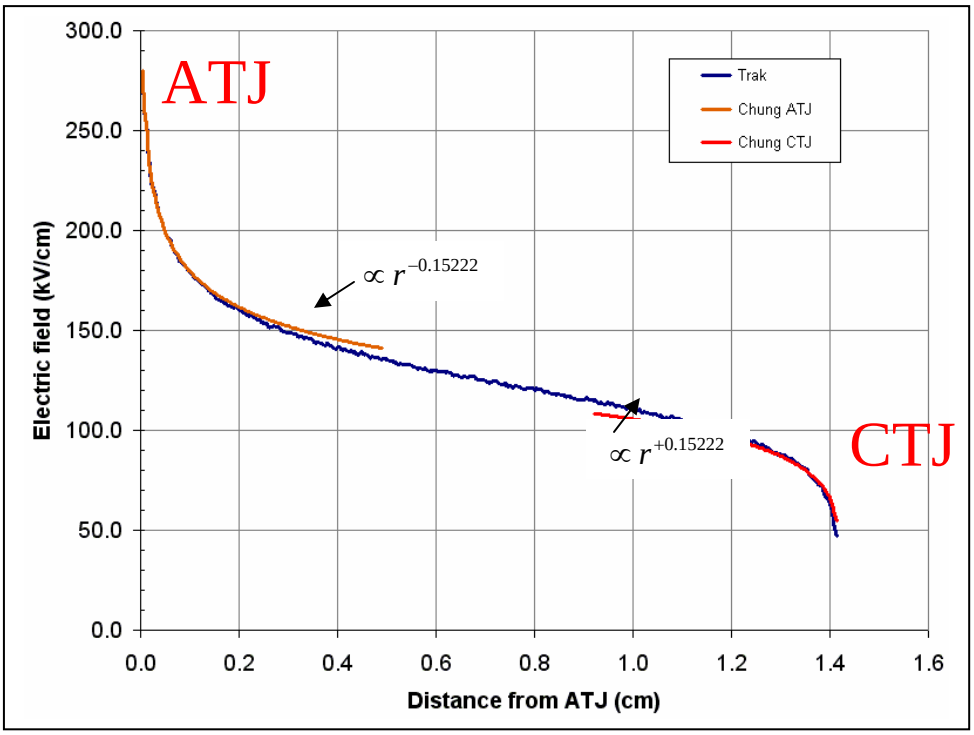

Zoom on ATJ and CTJ in ln-ln plot since:

$$E = Ar^{\nu-1} \rightarrow \ln(E) = (\nu-1)\ln(r) + \ln(A)$$

$$\rightarrow \quad y = m \quad x + b$$

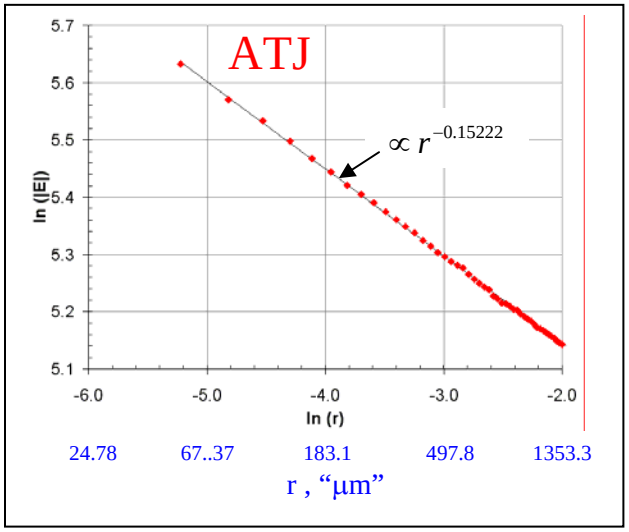

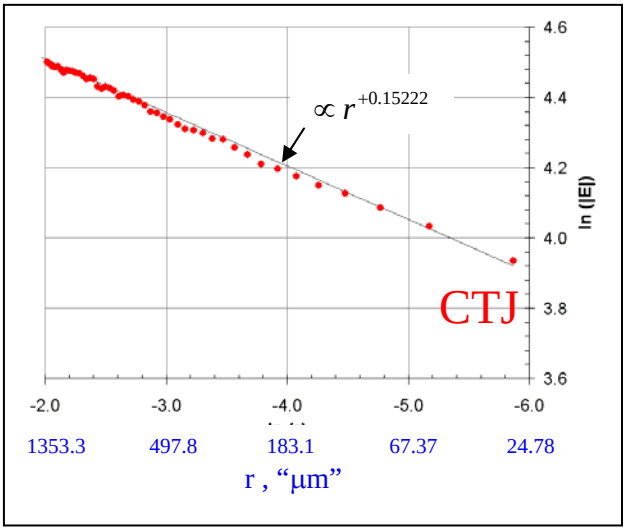

2) 0.2 μm mesh case: Zoom on ATJ and CTJ in ln-ln plot

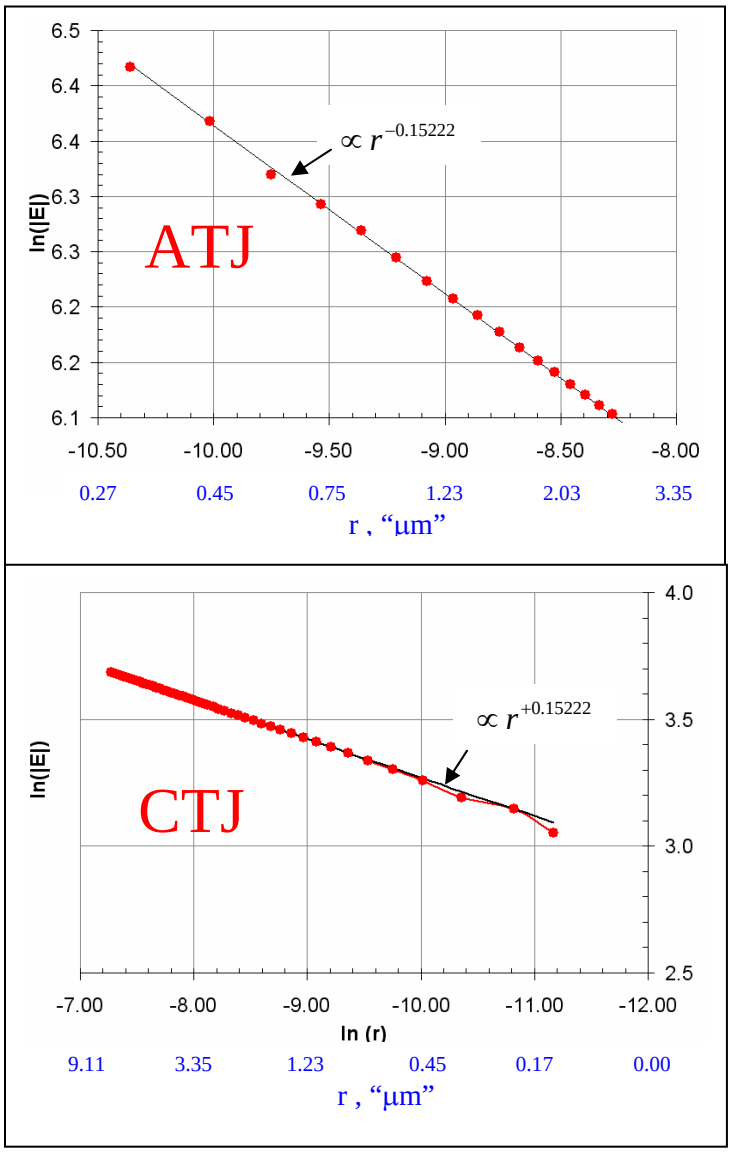

For the two cases of 30 μm and 0.2 μm mesh, the agreement between Trak (FEM Computational) and Chung's (Analytical) results is quantified in terms of % difference in |E|:

Mesh Size, μm	**Distance from ATJ, μm** $\%\Delta \lvert E \rvert$	**Distance from CTJ, μm %** $\%\Delta \lvert E \rvert$
30.0	$30\ \mu m \le r \le 1500\ \mu m$ 0.6%	$30\ \mu m \le r \le 2500\ \mu m$ 2.0%
0.2	$0.72\ \mu m \le r \le 1500\ \mu m$ 0.2%	$0.86\ \mu m \le r \le 2500\ \mu m$ 0.2%

The agreement for the 0.2 μm mesh case is within 0.2%.

Appendix 4: – Plasma Simulation with Trak and Coupling with Microcap

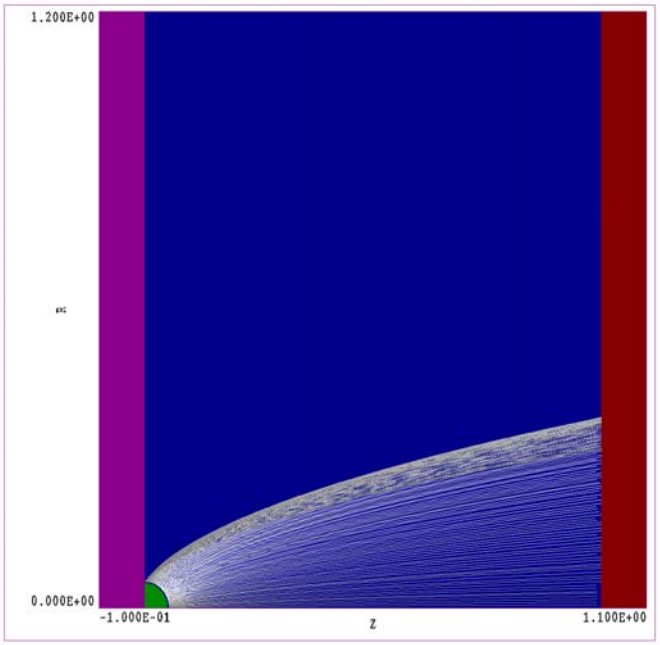

Time (ns)	Voltage (kV)	Current (A)
0	100	7.97
30	100	16.2
60	100	26.3
90	100	39
120	100	53
150	100	68
180	100	85.7
210	100	106
240	100	128.5
270	100	153.4
300	100	181.4
330	100	212.7
360	100	247.9
390	100	287.9
420	100	331.6
450	100	382
480	100	440.6
510	100	507.2
540	100	583.7
570	100	676.6
600	100	778.8
630	100	904.5
660	100	1058
690	100	1246
720	100	1485
750	100	1796
780	100	2221
810	100	2824
840	100	3755
870	100	5391
900	100	9049
930	100	24830

Figure A4-1: (a) Trak Sample output, showing electron trajectories cases that were run with Trak at later evolution of plasma in time.

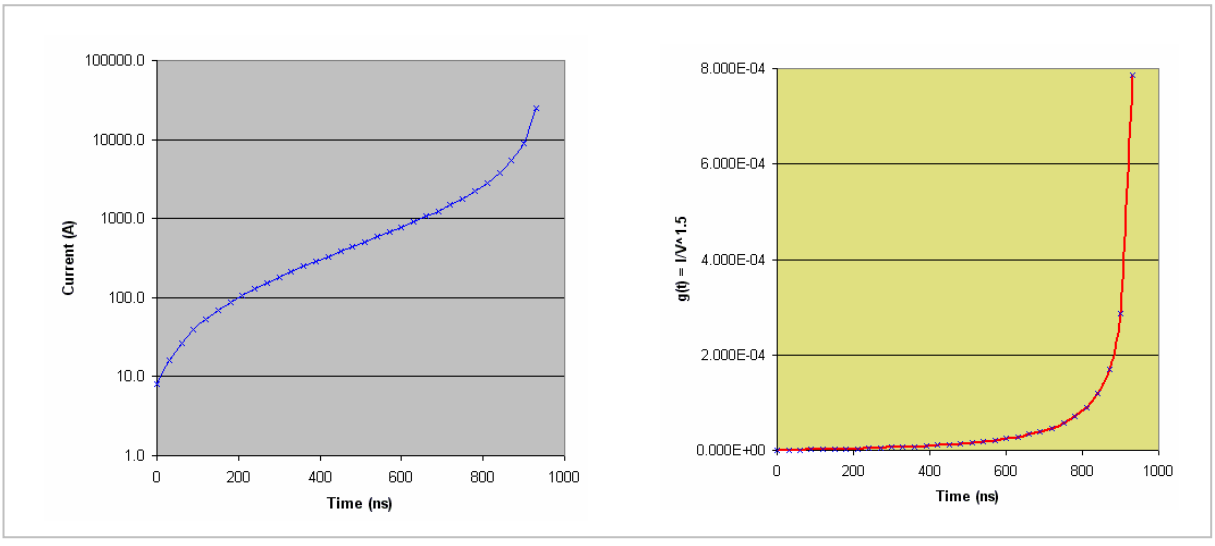

Figure A4-2: (a) Plot of Current vs Time for the expanding plasma from Trak runs (b) A plot of the geometrical factor g(t), vs. time. In the Microcap modeling of the circuit, since Voltage is known the plasma current is determined by: $I = g(t) * V^{1.5}$

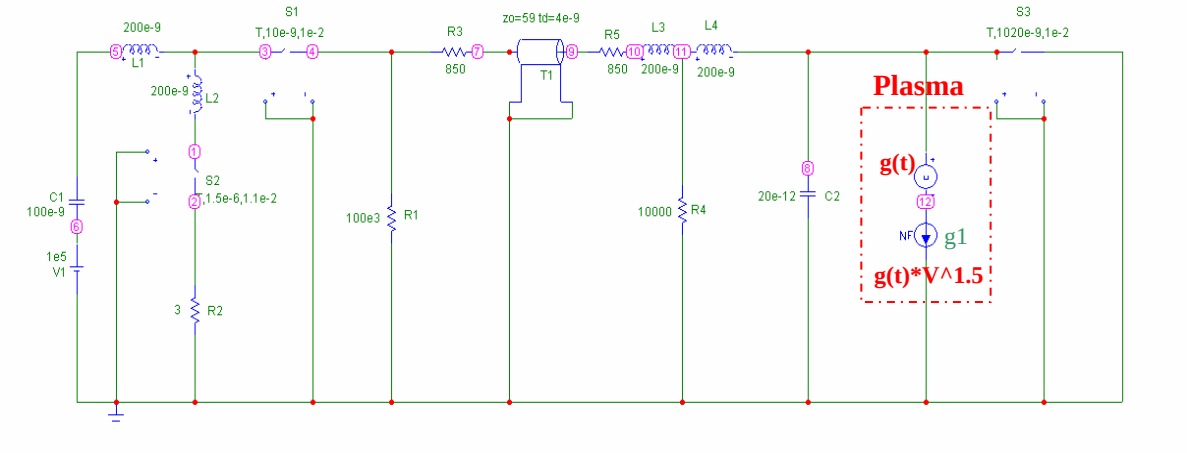

Figure A4-3: Applying g(t) to the circuit model in Microcap. First g(t) data set is read in as a user defined table and then NFI current source is used to multiply g(t) voltage which is (v[8]-v[12]) by V[8]^1.5.

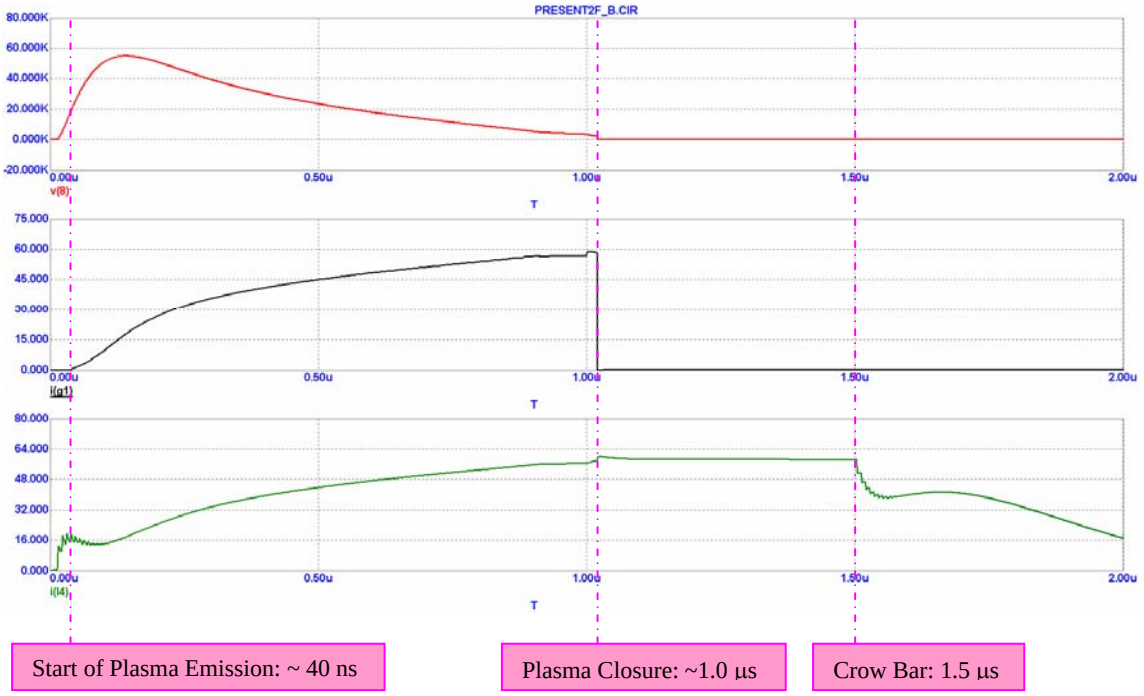

Figure A4-4: Output waveforms of the circuit model; showing the voltage across the insulator, plasma current, and the current picked up by the current probe.

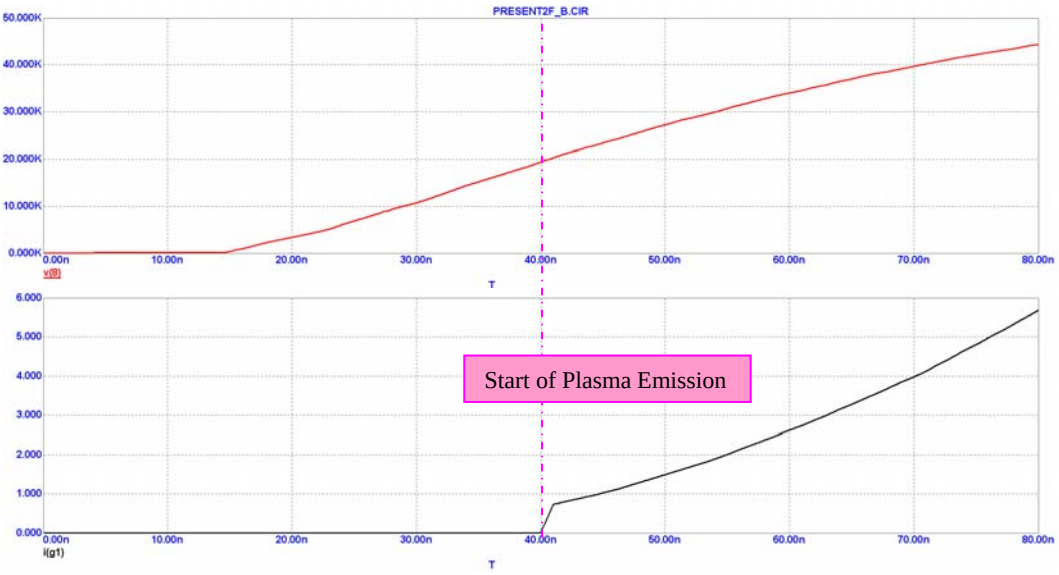

Figure A4-5: Output waveforms of the circuit model; Zoomed.

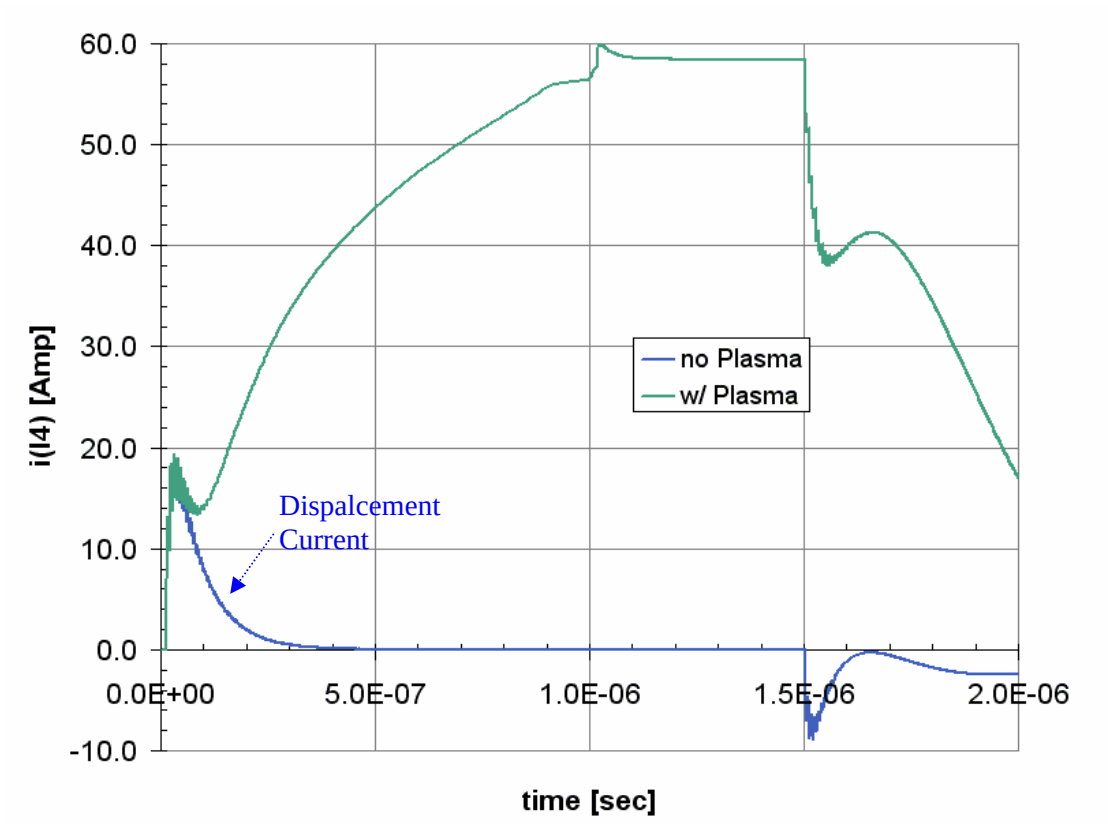

Figure A4-6: Shows the Current measured by the current probe with and without the plasma. The current for the no-plasma case is the capacitor's displacement current.

Appendix 5: – Electron Transit Time across the Gap

Assuming E_z is constant and is equal to: $E_z = \frac{V}{L}$ (1)

Where, V is the applied potential and L is the electrode spacing:

$$F_z = \frac{\partial P_z}{\partial t} = eE_z = e\frac{V}{L} \quad (2)$$

Integrating above;

$$\int \frac{\partial P_z}{\partial t} = \int \frac{eV}{L} \qquad \int_{P_i}^{P_f} dP_z = \frac{eV}{L}\int_0^T dT = \frac{eVt}{L} \quad (3)$$

Solving for transit time t:

$$\boxed{t = \frac{LP_f}{eV}} \quad (4)$$

1) Non-Relativistic Treatment:

$$P_z = mv$$

Where v is determined from: $\frac{1}{2}mv^2 = eV$ (5)

Equation (4) in this case is:

$$t_{NR} = \sqrt{\frac{2mL^2}{eV}} \quad (6)$$

For a typical case where $L = 1.0$ cm and $V = 20kV$:

$$t_{NR} = \sqrt{\frac{2*\left(0.511E+06/c^2\right)*0.01^2}{20E+03}} = 0.2383\ ns$$

2) Relativistic Treatment:

$$P_z = mc\sqrt{\gamma^2 - 1} \quad (7)$$

Where γ is derived from: $\gamma mc^2 = KE + mc^2 = eV + mc^2$ (8)

Equation (4) in this case is:

$$\boxed{t_R = \frac{L}{c}\sqrt{1 + \frac{2mc^2}{eV}}} \quad (9)$$

For an example case where $L = 1.0\,\text{cm}$ and $V = 20kV$:

$$t_R = \frac{0.01}{c}\sqrt{1+\frac{2*0.511E+6}{20E+03}} = 0.2406\ ns$$

Table 1: Free electron transit time for 1 cm

A Applied Voltage, [kV]	t_{NR} $[ns]$	t_R $[ns]$
20.0	0.2383	0.2406
40.0	0.1684	0.1718
60.0	0.1376	0.1416
80.0	0.1191	0.1237
100.0	0.1066	0.1165

Equations (6) and (9) can be reapplied for an ion (proton) where the only difference is mass which is 931 Mev/c^2

Table 2: Free ion transit time for 1 cm

Applied Voltage, [kV]	t_{NR} $[ns]$	t_R $[ns]$
20.0	10.17	10.17
40.0	7.19	7.19
60.0	5.87	5.87
80.0	5.09	5.09
100.0	4.55	4.55